

RESEARCH ARTICLE

Evaluation of multi-RCM ensembles for simulating spatiotemporal variability of Asian summer monsoon precipitation in the CORDEX-East Asia Phase 2 domain

Ga-Yeong Seo¹  | Joong-Bae Ahn²  | Dong-Hyun Cha³  |
Myoung-Seok Suh⁴  | Seung-Ki Min⁵  | Eun-Chul Chang⁴  |
Young-Hwa Byun⁶  | Jin-Uk Kim⁶ 

¹Department of Atmospheric Sciences,
Division of Earth Environmental System,
Pusan National University, Busan,
South Korea

²Department of Atmospheric Sciences,
Pusan National University, Busan,
South Korea

³Department of Urban and
Environmental Engineering, Ulsan
National Institute of Science and
Technology, Ulsan, South Korea

⁴Department of Atmospheric Sciences,
Kongju National University, Gongju,
South Korea

⁵Division of Environmental Science and
Engineering, Pohang University of
Science and Technology, Pohang,
South Korea

⁶Climate Change Research Team,
National Institute of Meteorological
Sciences, Seogwipo, South Korea

Correspondence

Joong-Bae Ahn, Department of
Atmospheric Sciences, Pusan National
University, Geumjeong gu, Busan 46241,
South Korea.

Email: jbahn@pusan.ac.kr

Funding information

Korea Meteorological Administration
Research and Development Program,
Grant/Award Number: KMI2020-01411

Abstract

Five regional climate models (RCMs)—CCLM, RegCM, HadGEM3-RA, SNURCM and WRF—participating in the Coordinated Regional Climate Downscaling Experiment-East Asia (CORDEX-EA) Phase 2 project are evaluated for their ability to simulate spatiotemporal variability in Asian summer precipitation. For this purpose, two dynamical downscaling sets, experiments forced by ERA-Interim reanalysis data (reproduction experiment) and historical data from three Coupled Model Intercomparison Project 5 (CMIP5) general circulation models (GCMs) (historical experiment) are analysed. The horizontal resolution of the downscaled results is 25 km, and the analysis period is from 1981 to 2005 (25 years). The RCMs show reasonable performance in simulating the spatial and temporal characteristics of summer precipitation in CORDEX-EA Phase 2 domain. To assess spatiotemporal patterns in Asian precipitation, cyclostationary empirical orthogonal function (CSEOF) analysis is used. In the first mode representing seasonal variations, the model ensemble results of both the reproduction experiment (Rep_ENS) and the historical experiment (His_ENS) simulate the peak times, location of precipitation and progression of the monsoons in Asia reasonably. Their features are greatly influenced by the moisture flux, indicating that the relation between precipitation and 850 hPa moisture flux is depicted well by RCM ensembles. In the second mode, which represents intraseasonal variations, the Rep_ENS depicts the western North Pacific summer monsoon break (WNPSM break) phenomenon similar to the observation. Although the His_ENS simulates the WNPSM break later than the observation, it does present the intraseasonal variation in the East Asian summer monsoon region. Based on these results, the five RCM ensemble results show the ability to capture spatiotemporal characteristics of summer precipitation in CORDEX-EA Phase 2 domain, as well as added value from dynamical downscaling.

This is an open access article under the terms of the [Creative Commons Attribution-NonCommercial](https://creativecommons.org/licenses/by-nc/4.0/) License, which permits use, distribution and reproduction in any medium, provided the original work is properly cited and is not used for commercial purposes.

© 2023 The Authors. *International Journal of Climatology* published by John Wiley & Sons Ltd on behalf of Royal Meteorological Society.

KEYWORDS

CORDEX-EA Phase 2, CSEOF, precipitation, regional climate model ensemble, spatiotemporal variability

1 | INTRODUCTION

Prediction ability for future climate change is determined by our understanding of current climate and climate modelling skills (Marsh et al., 2007). Numerous climate models have been developed and improved over the past few decades to analyse and predict atmospheric phenomena. The general circulation model (GCM), which simulates global climate, has helped us to respond to climate change by describing large-scale climate processes and making future projection possible (Huth et al., 2000; Wilby & Wigley, 2000; Yan et al., 2013). However, the coarse resolution used for the GCM makes it difficult to simulate regional-scale climates in detail (Ashfaq et al., 2010; Im et al., 2016). Hence, the regional climate model (RCM) has frequently been used in recent years to overcome the GCM's shortcomings and to adequately address regional characteristics of climate for a limited domain. Many studies have illustrated how RCMs enable simulations of local climatic events in any area by using high-resolution grids and appropriate physical parameterization (Afrizal & Surussavadee, 2018; da Rocha et al., 2009; Wang et al., 2014).

Recently, RCMs have been used to dynamically downscale GCM data under the Coordinated Regional Climate Downscaling Experiment (CORDEX). CORDEX is an international project producing fine-resolution climate datasets by using RCMs for 14 designated regions around the world (e.g., EURO-CORDEX, Med-CORDEX, CORDEX-EA and CORDEX-Africa). Numerous studies have presented various characteristics of current and future regional climate through this project (Ashfaq et al., 2020; Bartók et al., 2017; Li et al., 2018b; Mariotti et al., 2014; Ruti et al., 2016). Since different RCM experiments are designed under the CORDEX framework, CORDEX data enable a multimodel ensemble (MME) approach. In RCM MME experiments, several ensemble combinations are possible (e.g., one GCM–multi-RCM, multi-GCM–one RCM and multi-GCM–multi-RCM). Different dynamic and physical schemes used in each RCM as well as various forcing data contribute to large spreads in the MME results. MME gives us a significant climate signal despite uncertainties, and better ensemble combinations and optimal ensemble methods for the signals are still under debate (Déqué et al., 2007; Xue et al., 2014). However, MMEs have demonstrated better performance than individual models, enhancing the reliability of future climate projections (Diallo et al., 2012; Herrera et al., 2010; Im et al., 2016; IPCC, 2013). Regarding the CORDEX project, previous studies analysed the regional climate in different parts of the world by using multimodel

ensembles of the CORDEX data (Berg et al., 2019; Dosio, 2016; Fantini et al., 2018; Tangang et al., 2020). For example, Berg et al. (2019) analysed subdaily extreme precipitation in several European countries during the summer using a EURO-CORDEX data ensemble. Tangang et al. (2020) examined multi-GCM and multi-RCM ensemble performance for simulating current precipitation and projected future rainfall changes over Southeast Asia. These studies led to a better understanding of local climate phenomena using CORDEX MME data. Along this line, CORDEX-East Asia (CORDEX-EA) ensemble data produced by multiple GCMs–multiple RCMs chains are utilized in this study for evaluation of the summer monsoon in terms of precipitation.

Several studies simulated the historical and future climate for the CORDEX-EA Phase 1 domain based on RCP scenarios using multi-RCMs and analysed in several studies (Gu et al., 2018; Huang et al., 2015; Jin et al., 2016; Kim et al., 2021; Lee et al., 2019; Li et al., 2018a; Oh et al., 2013; Park et al., 2013; Park & Min, 2019; Zou et al., 2016). The RCM performance and projecting future climate change were evaluated by downscaling reanalysis data (ERA-Interim and NCEP/DOE2) and the Coupled Model Intercomparison Project 5 (CMIP5) GCM data under CORDEX-EA Phase 1 project. Oh et al. (2013) examined influences of different boundary conditions on extreme climate using RegCM, and Kim et al. (2021) projected mean and extreme precipitation changes with a multimodel ensemble. Recently, CORDEX-EA Phase 2 experiments were conducted with a 25-km spatial resolution to produce a more detailed Asian climate simulation than from the Phase 1 experiment domain with a 50 km resolution (Jo et al., 2019; Lee et al., 2020; Wang et al., 2021; Yu et al., 2020; Zou & Zhou, 2022). Research assessing the RCM performance, correcting for systematic errors and projecting regional climate change for the new domain is still underway.

Atmospheric phenomena with various temporal and spatial scales can be identified by analysing regional climate model simulations (Kim et al., 2021). The most distinguishing phenomenon in this region is the Asian summer monsoon (ASM). The ASM involves complicated dynamic and thermodynamic processes that include interaction and feedback among various climate factors, such as atmospheric and oceanic circulations and land–sea contrast (Fu & Zeng, 1997; Liu et al., 2015; Tang et al., 2017). Variations in the ASM related to climate change can have a huge impact on socio-economic sectors, because it significantly influences activities in the habitats of the region and, in some cases, brings severe economic

and human loss (Li et al., 2019). Hence, several regional climate model experiments have been conducted for adequate understanding and prediction of the ASM, especially in terms of precipitation (Bhaskaran et al., 1996; Gao et al., 2008; Kang & Hong, 2008; Lee & Suh, 2000; Li et al., 2016). Kang and Hong (2008) showed the effect on the East Asian summer monsoon (EASM) simulation ability from using four different cumulus parameterization schemes in an RCM. They showed that an RCM has the ability to reproduce precipitation patterns that are not represented by the GCM and showed that it is a suitable tool for simulating local climate features in Asia characterized by complex topography (Gao et al., 2008; Liu et al., 1994).

In this study, we evaluate the performance of five RCMs simulating spatiotemporal characteristics of summer precipitation over the CORDEX-East Asia Phase 2 domain. Multi-RCMs are forced by multi-GCMs: ERA-Interim reanalysis and CMIP5 data. This study focuses on three major ASM regions (Northeast Asia, India and the western North Pacific) where complicated precipitation characteristics and distinct life cycles appear. The summer monsoon in Northeast Asia can be described as a meridional advance of a stagnant rainy front called Changma in Korea, Meiyu in China, Baiu in Japan or the BCM front (Chu et al., 2012; Hong & Ahn, 2015; Noh et al., 2020; Park et al., 2020). The interannual variability of the western North Pacific subtropical high plays a crucial role in the movement of EASM rainfall (Chang et al., 2000; Lee et al., 2013; Lu, 2001). The EASM has a negative correlation with the western North Pacific summer monsoon (WNPSM) (Kwon et al., 2005; Wang et al., 2001), which is described as a monsoon trough oriented northwest-to-southeast and dominantly affected by sea surface temperature (Li & Wang, 2005; Murakami & Matsumoto, 1994). It is well known that the WNPSM has various timescales, ranging from intraseasonal to interdecadal, where its interannual variability is closely related to the ENSO, and intraseasonal variability of the WNPSM regulates the locations of tropical cyclone genesis (Li & Wang, 2005; Wang et al., 2001). For the Indian summer monsoon (ISM), rainfall-producing mechanisms are explained by a northward propagating 30–60 days of intraseasonal oscillation and a westward propagating 10–20 days of intraseasonal oscillation (Ding & Wang, 2007; Suhas & Goswami, 2008). In addition, ISM rainfall is characterized separately in several different subregions (Cash et al., 2015; Dash et al., 2009). Since the ASM has multiple temporal and spatial variability spectrums as it interacts with various climate patterns (Ding, 2007; Ha et al., 2012; Hrudya et al., 2020), understanding ASM rainfall variability is crucially important when studying climate variability and changes in the region.

In order to analyse an RCM's ability to simulate spatiotemporal monsoon precipitation patterns, the

cyclostationary empirical orthogonal function (CSEOF) method is utilized (Kim et al., 1996). The CSEOF is one of the statistical methods decomposing a dataset into a distinct spatiotemporal progress mode. Most climate variables evolve in time and space following their own internal cycles. Therefore, the CSEOF can be a proper tool to extract the physical evolution of weather events, whereas empirical orthogonal function (EOF) analysis presents a time-independent spatial pattern (Hamlington et al., 2014; Kim & Kim, 2004). Annamalai and Sperber (2005) analysed boreal summer intraseasonal variability with the CSEOF method and presented the connections among the components of summer intraseasonal variability. Lim et al. (2002) analysed the space–time evolution of the observed ASM and the associated synoptic fields using a CSEOF technique. The CSEOF also can be a useful method to find out the capability of a numerical model in simulating climate variability (Bergant et al., 2007; Hong & Ahn, 2015; Im et al., 2007; Shin et al., 2010). The aim of this study is to evaluate RCM performance in terms of both temporal and spatial characteristics of ASM precipitation over the whole CORDEX-EA Phase 2 domain using the CSEOF method utilizing multi-GCM–multi-RCM matrix chains.

This paper is structured as follows. Model descriptions and setups, observation data and methods are described in section 2. Evaluation of the results from individual models and the RCM MME with respect to the spatiotemporal characteristics of precipitation are shown in section 3. Improvements to the RCM, compared to the GCM, for simulating precipitation are also explained. The summary and conclusion are in section 4.

2 | DATA AND METHODS

2.1 | Model description and observation

Five regional climate models (CCLM, RegCM, HadGEM3-RA, SNURCM and WRF) are employed in this study to simulate the Asian summer climate. Among them, RegCM is a hydrostatic model, and the others are nonhydrostatic models. Simulations are conducted under the CORDEX-EA Phase 2 domain with the 25-km horizontal resolution (Figure 1). This domain covers the Asian-Pacific summer monsoon regions and 85% of tropical cyclone activity over the western North Pacific (Lee et al., 2020). Different physical parameterization schemes utilized for each RCM and detailed model configuration are provided in Table 1. For the reproduction experiment, all five RCMs are forced by ERA-Interim reanalysis data with $0.75^\circ \times 0.75^\circ$ horizontal resolution from the European Centre for Medium-Range Weather Forecasts (ECMWF) (Simmons et al., 2007) for the lateral boundary condition (LBC). A simple composite method that gives the same weight to all model data is used

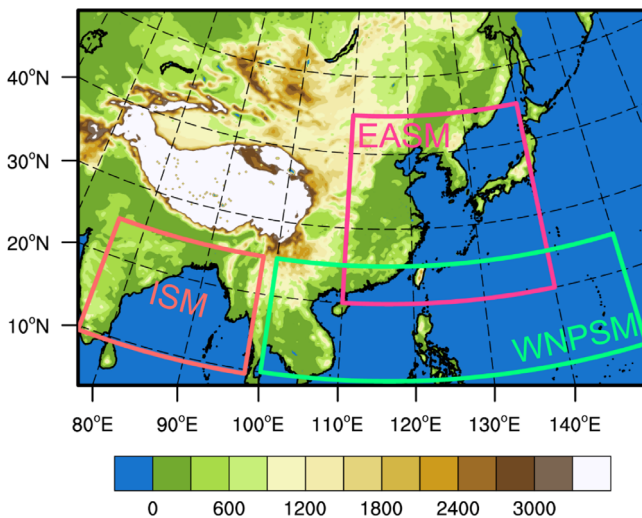


FIGURE 1 Topography (unit: m) of the CORDEX-East Asia Phase 2 domain [Colour figure can be viewed at wileyonlinelibrary.com]

for RCM MMEs, and the ensemble results of the reproduction experiment are denoted Rep_ENS.

The historical experiment is conducted using a combination of three GCMs from CMIP5 and five RCMs that have the same configuration as the RCMs used in the reproduction experiment. Each RCM conducts two historical scenario experiments with different boundary condition data. Overall, the historical experiment consists of 10 model results with two GCM boundary conditions per RCM. The three CMIP5 GCMs used in this study include the Hadley Centre Global Environmental Model version 2—Atmosphere and Ocean (HadGEM2-AO), which has a 1.25° (lat) \times 1.875° (lon) horizontal resolution and 38 vertical layers (Baek et al., 2013). CCLM, HadGEM3-RA, SNURCM and RegCM use HadGEM2-AO as the LBC. Also used is the Max Planck Institute Earth System Model, Low Resolution (MPI-ESM-LR) GCM, which has a $1.9^\circ \times 1.9^\circ$ horizontal resolution and 47 vertical layers (Giorgetta et al., 2013). CCLM, HadGEM3-RA, SNURCM and WRF use the MPI-ESM-LR GCM. Third is the Geophysical Fluid Dynamics Laboratory Earth System Model, version 2M (GFDL-ESM2M) (Dunne et al., 2012) with a 2.0° (lat) \times 2.5° (lon) resolution as the LBC for RegCM and WRF. We average 10 historical experiment sets of data using an MME method, denoting the results as His_ENS. The reproduction experiment conducts modelling experiment from 1979 to 2015, while the historical experiment conducts modelling experiment from 1979 to 2005. To match the same periods, an analysis is done for the 1981–2005 period (25 years), while the 1979–1980 period is regarded as spin-up time.

Assuming that ERA-Interim data are “perfect,” the data are used as observation for model verification. That

enables to estimate of systematic error in the reproduction experiment results and examine of performance from the historical experiment. In addition to ERA-Interim, various types of precipitation observation data are utilized, such as Asian Precipitation-Highly Resolved Observational Data Integration Towards Evaluation of the Water Resources (APHRODITE) (Yatagai et al., 2012), Modern-Era Retrospective Analysis for Research and Applications, Version 2 (MERRA2) (Gelaro et al., 2017) and Climatic Research Unit (CRU) (Harris et al., 2014). Data interpolation is conducted for comparison with the observation and consistency of results in the CSEOF analysis. The high-resolution RCM data are interpolated bilinearly into the ERA-Interim grid to prevent distortion of the coarse-resolution validation data (Hong & Kanamitsu, 2014; Merino et al., 2021; Prein & Gobiet, 2017). According to Torma et al. (2015) and Qiu et al. (2020), the added values of RCM remain and are not significantly degraded in the upscaled grid when the interpolation is used.

We defined three summer monsoon areas in Asia (Wang & Ho, 2002) to analyse regional monsoons in terms of precipitation (Figure 1). Although the whole target region is the CORDEX-East Asia Phase 2 domain, the region is divided into three monsoon areas: ISM, EASM and WNPSM regions where the respective Indian, East Asian and western North Pacific summer monsoons appear.

2.2 | The performance index

A performance index (PI) is employed as an objective value to determine agreement between models and observations (Baek et al., 2013; Reichler & Kim, 2008). The PI is a relative index that assesses how good the model performance is compared to the average performance. First, normalized error variance (E^2) is obtained by subtracting the observed value from a single-model value, dividing it by the standard deviation of the observation for each grid, then squaring it, and averaging all grid points,

$$E^2 = \sum_{n=1}^N w_n \left(\frac{\bar{s}_n - \bar{o}_n}{\sigma_{n,o}} \right)^2 \quad (N = \text{number of grid points}), \quad (1)$$

where \bar{s}_n and \bar{o}_n represent the climatology for the grid points of models and observations, w_n denotes proper weights needed for area averaging and $\sigma_{n,o}$ denotes the standard deviation over time from the observations.

Then, the PI (I^2) is calculated by dividing E_r^2 into the averaged E_a^2 for all RCMs and averaging for all the variables, where E_r^2 and E_a^2 represent E^2 for the specific region and the entire domain, respectively,

TABLE 1 Regional climate model configurations

Model	CCLM	HadGEM3-RA	RegCM	SNURCM	WRF
Domain	CORDEX-East Asia Phase 2 (25 km)				
Analysis period	1981–2005 (25 years)				
LBC for reproduction experiment	ERA-Interim				
LBC for historical experiment	HadGEM2-AO MPI-ESM-LR	HadGEM2-AO MPI-ESM-LR	HadGEM2-AO GFDL-ESM2M	HadGEM2-AO MPI-ESM-LR	MPI-ESM-LR GFDL-ESM2M
Vertical layers	40 hybrid	63 eta	23 sigma	24 sigma	30 eta
Cumulus	Tiedtke (Tiedtke, 1989)	Revised mass flux (Grant & Brown, 1999; Gregory & Rowntree, 1990)	MIT-Emanuel (Emanuel, 1991)	Kain-Fritsch (Kain, 2004)	Betts-Miller-Janjic (Betts & Miller, 1986; Janjić, 1994)
Microphysics	Extended DM (Seifert & Beheng, 2001)	Single moment bulk (Wilson & Ballard, 1999)	SUBEX (Pal et al., 2000)	Reisner2 (Reisner et al., 1998)	WSM3 (Hong et al., 2004)
Radiation	Ritter and Geleyn (Ritter & Geleyn, 1992)	General2 (Cusack et al., 1999; Edwards & Slingo, 1996)	NCAR CCM3 (Kiehl et al., 1996)	CCM2 package (Briegleb, 1992)	CAM (Collins et al., 2002)
Land surface	TERRA ML (Schrodin & Heise, 2002)	JULES (Best et al., 2011)	NCAR CLM3.5 (Oleson et al., 2008)	NCAR CLM3 (Bonan et al., 2002)	NOAH-LSM (Chen & Dudhia, 2001)

$$I^2 = \frac{1}{L} \sum_{v=1}^L \left(\frac{E_r^2}{\frac{1}{K} \sum_{m=1}^K (E_a^2)_m} \right)_v, \quad (2)$$

where K is the number of RCM and L is the number of variables.

Therefore, the PI means the error in the specific model normalized by averaging the errors for all models for all domains. The lower I^2 is preferred, and an index lower than 1.0 means the model performs relatively better than average (Baek et al., 2013). In this study, 17 variables are used to calculate the PI, and specific variables—surface temperature (ts), surface upward latent heat flux (hfls), surface downwelling shortwave radiation (rsds) and near-surface wind speed (sfcWind)—which four out of five RCMs have, are included in the calculation (Table 2).

2.3 | Cyclostationary empirical orthogonal function

The cyclostationary empirical orthogonal function is a useful technique for extracting time-dependent spatial

modes of physical phenomena (Kim et al., 1996; Kim et al., 2018; Kim & North, 1997; Lim & Kim, 2007). Climate data ($M(r, t)$) in the CSEOF are expressed as follows:

$$M(r, t) = \sum_{n=1} B_n(r, t) T_n(t), \quad (3)$$

where $B_n(r, t)$ is the cyclostationary loading vector (CSLV) for the n th mode, which is a function of time (t) and space (r), and $T_n(t)$ represents the principal component (PC) time series of the n th mode. In CSEOF analysis, CSLVs are periodic in time,

$$B_n(r, t) = B_n(r, t + d), \quad (4)$$

where d is the nested period and number of d CSLVs for each mode is produced through CSEOF analysis. In this study, CSEOF is applied to 5-day mean (pentad mean) precipitation data from 11 May to 7 September, and the nested period is set to 24 ($t = 600, d = 24$). Then, the CSEOF loading vector describes temporal evolution of spatial patterns in the summer and the PC time series represents long-term variations in amplitude.

	CCLM	HadGEM3-RA	RegCM	SNURCM	WRF
tas	o	o	o	o	o
tasmax	o	o	o	o	o
tasmin	o	o	o	o	o
pr	o	o	o	o	o
psl	o	o	o	o	o
hus850	o	o	o	o	o
ta850	o	o	o	o	o
ua850	o	o	o	o	o
va850	o	o	o	o	o
zg500	o	o	o	o	o
ta200	o	o	o	o	o
ua200	o	o	o	o	o
va200	o	o	o	o	o
ts	–	o	o	o	o
hfls	o	o	–	o	o
rsds	o	o	–	o	o
sfcWind	o	o	–	o	o

TABLE 2 List of variables used for the performance index

CSLV is defined as a solution of the Karhunen–Loève equation (Loève, 1978):

$$C(r, t; r', t') B_n(r', t') = \lambda_n B_n(r', t'), \quad (5)$$

where $C(r, t; r', t')$ is a covariance function of the data and λ_n is an eigenvalue. Thus, variance in n th mode is $\sum_{i=1}^{\lambda_n} \lambda_i$.

The CSEOF analysis is conducted for precipitation and moisture flux at 850 hPa over the CORDEX-EA Phase 2 region. However, two sets of the CSEOF computed for two variables independently may not be consistent with each other (Lim & Kim, 2007). Therefore, regression is carried out to identify physically consistent modes among different variables (Hamlington et al., 2012; Kim et al., 2019; Lim & Kim, 2007). In this study, 850 hPa moisture flux is regressed to precipitation to show moisture flux at 850 hPa relevant to precipitation in the summer period. First, the PC time series of the first few significant modes of a predictor (moisture flux at 850 hPa) are regressed to a PC time series of the target variable (precipitation),

$$\text{PCT}_{pr,n}(t) = \sum_i \alpha_i \text{PCT}_{qv,i}(t) + \varepsilon(t), \quad (6)$$

where $\text{PCT}_{pr,n}$ and $\text{PCT}_{qv,i}$ are the PC time series of the n th mode for precipitation and the i th mode for moisture flux at 850 hPa, and α_i represents regression coefficients for each mode. We use the first 20 PC time series for moisture flux at 850 hPa and regress them to CSEOF modes 1 and 2 for precipitation, respectively. As a result,

the coefficient of determination (R^2) for mode 1 precipitation is 0.943, 0.973, 0.913 for zonal moisture flux, and 0.929, 0.973, 0.913 for meridional moisture flux in ERA-Interim, Rep_ENS and His_ENS, respectively. For mode 2, both zonal and meridional moisture flux are greater than 0.99 in all three data, so all variables show a close regression fit with each precipitation mode. Next, using the regression coefficients, the regressed CSLV for moisture flux can be written as

$$\text{RCSLV}_{qv,n}(r, t) = \sum_i \alpha_i \text{CSLV}_{qv,i}(r, t), \quad (7)$$

where $\text{CSLV}_{qv,i}(r, t)$ is the i th mode of the CSLV for moisture flux at 850 hPa and $\text{RCSLV}_{qv,n}(r, t)$ is the CSLV fit to the n th mode of the target variable through regression. Now, we can say that $\text{CSLV}_{pr,n}(r, t)$ and $\text{RCSLV}_{qv,n}(r, t)$ are physically and dynamically consistent with each other.

3 | RESULTS

The climatology of precipitation as derived from model results and observations is analysed to evaluate the skill of RCMs in simulating spatial characteristics of Asian summer precipitation. Figure 2 presents the spatial distributions of summer (May–September; MJJAS) mean precipitation and the bias obtained from reproduction experiments. For ERA-Interim, regions of heavy precipitation are distributed over latitudes below 30°N (Figure 2a). When compared to other observation data,

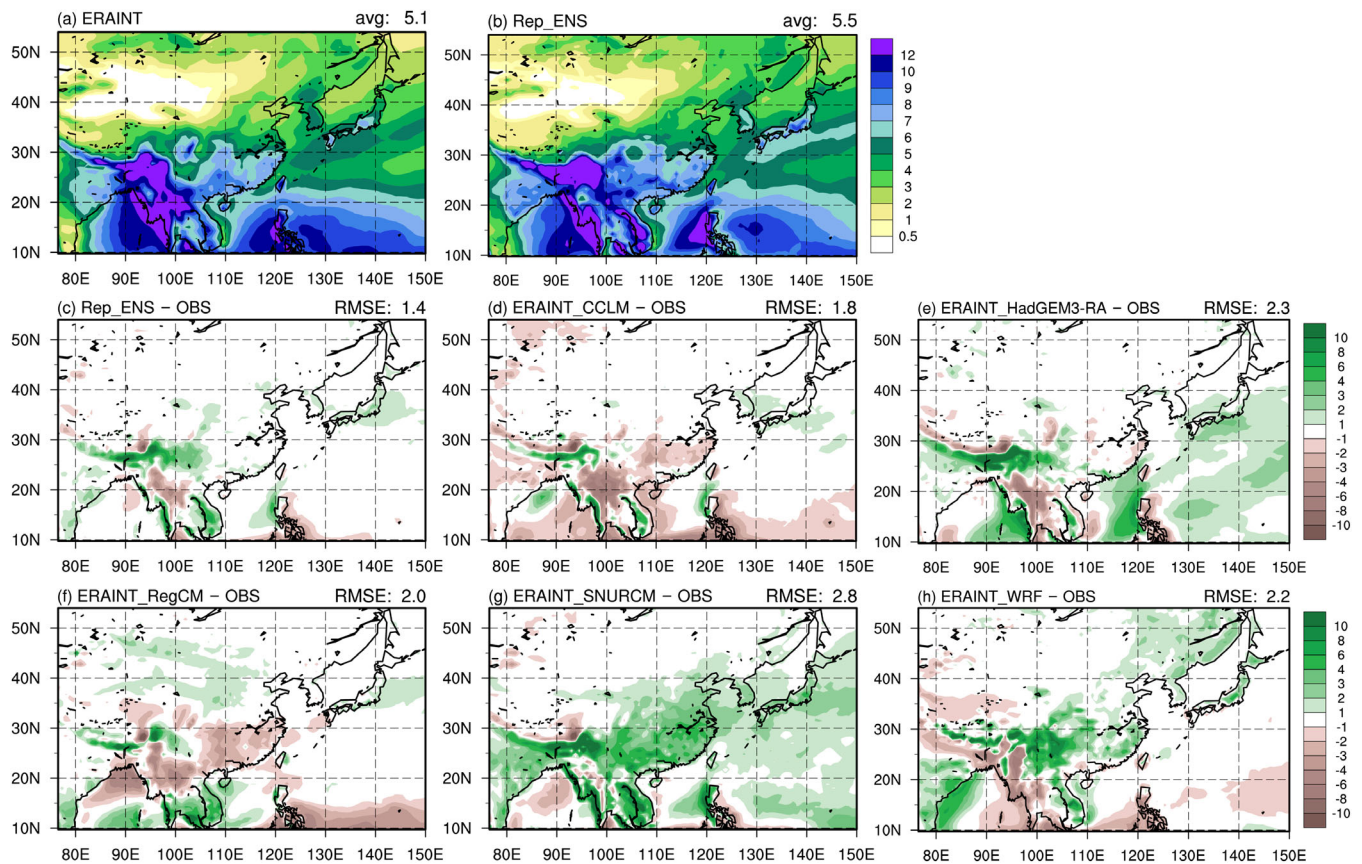


FIGURE 2 Spatial distributions of summer (MJJAS) mean precipitation (unit: $\text{mm}\cdot\text{day}^{-1}$) derived from (a) ERA-Interim, (b) the reproduction experiment RCM ensemble (Rep_ENS) and the differences between (c) Rep_ENS and ERA-Interim and (d–h) individual RCMs and ERA-Interim. Right upper text of each figure denotes the area-averaged (a–b) precipitation and (c–h) RMSE [Colour figure can be viewed at [wileyonlinelibrary.com](https://onlinelibrary.wiley.com)]

the large differences appear in that region indicating uncertainty in precipitation (Figure S1f–h). The mean precipitation distribution in Rep_ENS (Figure 2b) is similar to ERA-Interim. Rep_ENS simulates quite well the precipitation of more than $6 \text{ mm}\cdot\text{day}^{-1}$ over the land area below 30°N , and precipitation distribution over the Korean Peninsula and eastern China where the EASM occurs. As a result, spatial distribution of Rep_ENS shows small systematic error in most of the region (Figure 2c). However, Rep_ENS result overestimates precipitation in the Himalayas, southwestern China, the Korean Peninsula and Japan, and the similar results are also shown when compared with other observations (Figure S1i–l). Looking at the precipitation bias distribution of every single RCM, their patterns are somewhat different from each other because of the different dynamical processes and physical parameterizations in each RCM. However, all models show noticeable wet bias near the Himalayas (Figure 2c–h). This wet bias is one of the common problems in RCM simulations, for example, MM5 model, which is the original version of the SNURCM (Ratnam & Kumar, 2005), RegCM (Dash et al., 2006) and others (Janes et al., 2019; Saeed et al., 2009). One possible reason

is the excessive convergence in RCM simulation along the steep southern slopes of the Himalayas (Karmacharya et al., 2017). Both SNURCM and WRF show wet bias in most of the land areas, especially the region affected by the ASM (India, eastern China, the Korean Peninsula and Japan). On the other hand, CCLM and RegCM present dry bias over eastern China. HadGEM3-RA results show bias of less than $1 \text{ mm}\cdot\text{day}^{-1}$ in most of the land areas except the Himalayas (Indochina Peninsula), where wet (dry) bias is shown. RCMs for reproduction experiments simulate summer precipitation reasonably well overall, and in particular, Rep_ENS shows better performance than any other single RCM.

Systematic error of other variables in the summer period derived from individual RCMs and Rep_ENS are estimated using a PI (Figure 3). Most RCMs show relatively good simulation performance in Northern Asia (NAS), the Korean Peninsula (KOR), Japan (JPN), South-eastern Asia (SEA) and the Pacific Ocean region (NP, TP) by having PIs lower than 1.0. However, the results are different for each model in the east China (ECH), India (SAS) and the tropical Indian Ocean (TI) region and all five RCMs show a limited capability over the Tibet

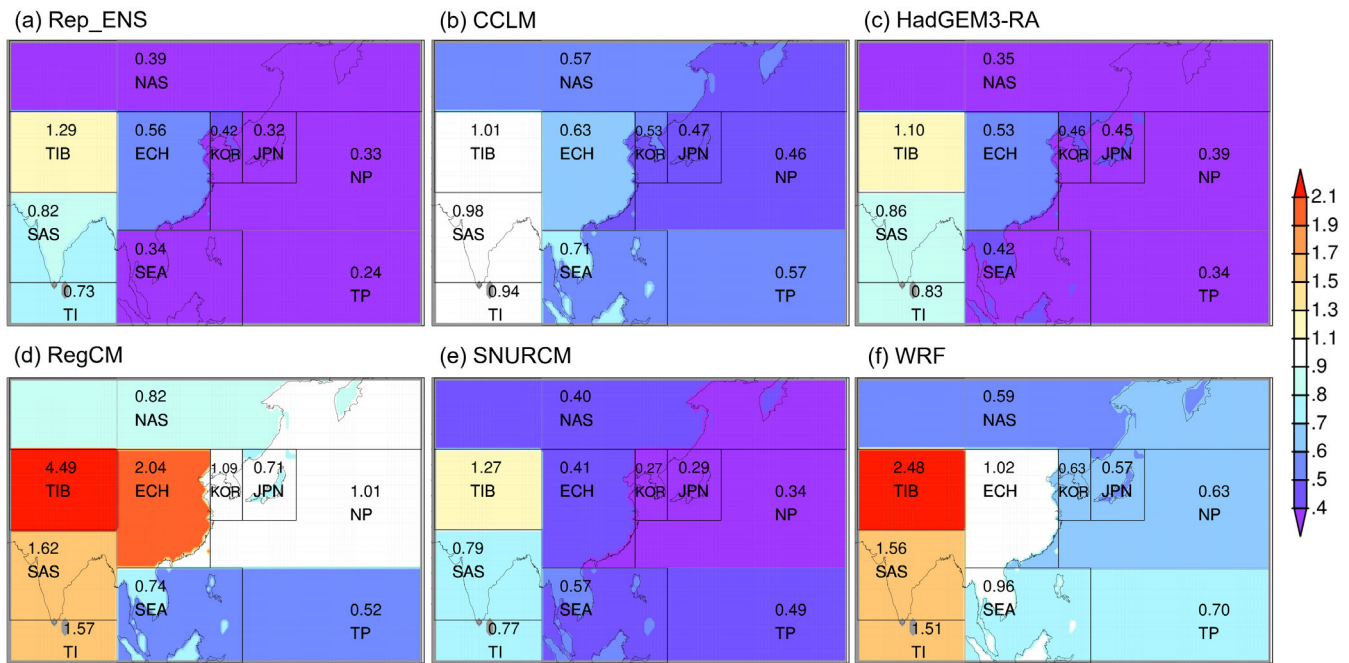


FIGURE 3 Performance index over CORDEX-East Asia Phase 2 domain in summer (MJJAS) derived from (a) the reproduction experiment RCM ensemble and (b–f) each of the five RCMs [Colour figure can be viewed at [wileyonlinelibrary.com](https://onlinelibrary.wiley.com/doi/10.1002/joc.8054)]

Plateau (TIB). Rep_ENS presents remarkable performance in most of the regions (Figure 3a). The PI is less than 1.0 in all areas except for TIB, and its improvement stands out compared to single RCMs. In simulating the ASM for summer monsoon regions (EASM, ISM and WNPSM) as defined in Figure 1, the results of the regional climate model ensemble are shown to be most appropriate.

Figure 4 illustrates spatial patterns of summer mean precipitation and the bias for the historical experiment. Overall, ensemble of RCM historical experiment (His_ENS; Figure 4c) represents spatial characteristics of precipitation in more detail, compared to the CMIP5 GCM ensemble (CMIP5 GCM_ENS), an ensemble of three GCMs forcing data (Figure 4b). His_ENS can capture observed precipitation distributions in areas with major mountain ranges (e.g., the Tibet Plateau, the Himalaya Mountains and mountains on the Indochina Peninsula). In particular, precipitation of more than $6 \text{ mm}\cdot\text{day}^{-1}$ for the northeastern region of India, which is not simulated in the CMIP5 GCM_ENS, is well captured in His_ENS, indicating added value based on use of RCM. The advantage obtained using the RCM is due mainly to its ability to resolve complex topography and coastlines (Feser et al., 2011; Giorgi, 2006; Torma et al., 2015). Compared to the CMIP5 GCM_ENS, bias diminishes in His_ENS over the Korean Peninsula and western part of the Indochina Peninsula (Figure 4e,f). The mean RMSE of His_ENS is lower than CMIP5 GCM_ENS for the land area (His_ENS: 1.62, CMIP5

GCM_ENS: 1.70), but the opposite result is observed for the entire domain due to an overestimation of precipitation in the western North Pacific. The southwest-to-northeast-oriented wet bias below Japan appears in CMIP5 GCM_ENS and His_ENS, indicating the influences of forcing data. The overestimated precipitation between 10°N and 20°N in the western North Pacific is also shown in other RCM simulation results (Kim et al., 2021; Oh et al., 2014). Since the RCM is the atmospheric climate model without ocean coupling, a limitation of representing air–sea interaction might lead to the wet bias in the ocean.

Most of the individual RCMs generally show wet bias (dry bias for RegCM) and larger RMSE than His_ENS, indicating advantage of RCM ensemble (Figure S2). Three RCMs (CCLM, HadGEM3-RA and RegCM) tend to underestimate summer precipitation on the Indochina Peninsula, in eastern China and on the Korean Peninsula. In experiments in which HadGEM2-AO (HG2) results are downscaled, dry bias is shown in most of the India and Indochina Peninsula regions (Figure S2a–d). For MPI-ESM-LR (MPI) and GFDL-ESM2M (GFDL) forcing experiment results (Figure S2e–j), wet (dry) are shown in southern India and the Japan (Tibet Plateau).

To evaluate the performance of individual RCMs and their ensembles when simulating spatial distributions of summer precipitation in terms of EASM, ISM and WNPSM in CORDEX-EA Phase 2 domain based on subdivided regions, Taylor diagrams are used (Taylor, 2001)

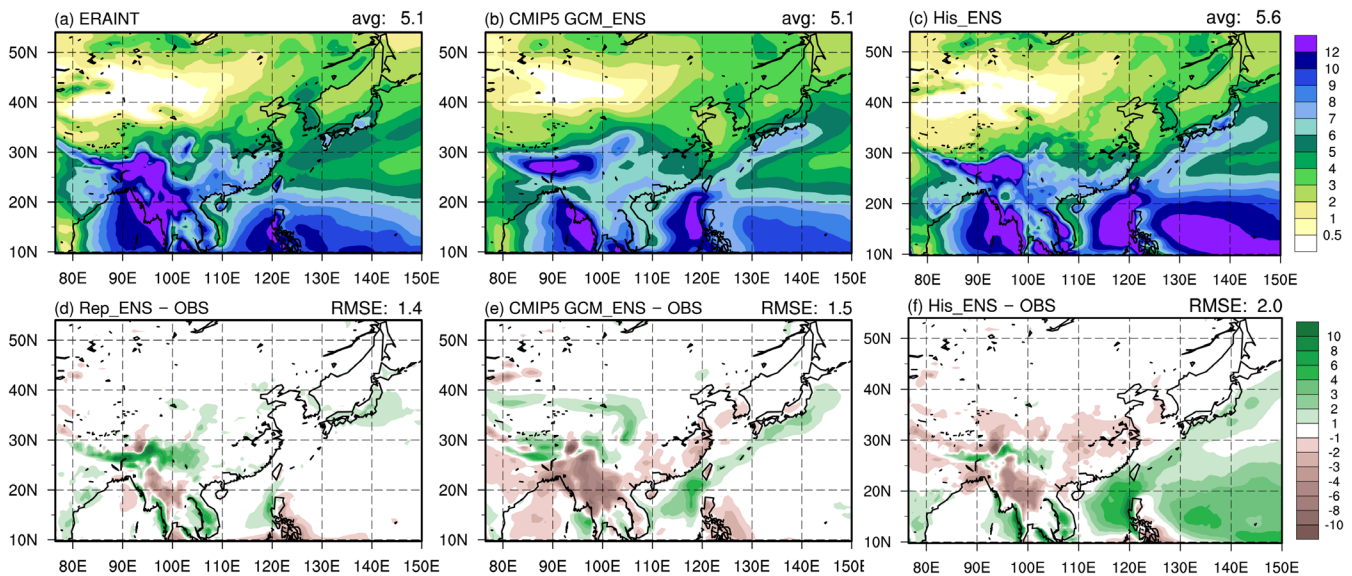


FIGURE 4 Spatial distributions of summer (MJJAS) mean precipitation (unit: $\text{mm}\cdot\text{day}^{-1}$) derived from (a) ERA-Interim, (b) CMIP5 GCM ensemble and (c) the historical experiment RCM ensemble (His_ENS), and the differences between (d) Rep_ENS and ERA-Interim, (e) CMIP5 GCM ensemble and ERA-Interim, (f) His_ENS and ERA-Interim. Right upper text of each figure denotes the area-averaged (a–c) precipitation and (d–f) RMSE [Colour figure can be viewed at wileyonlinelibrary.com]

(Figure 5). Spatial standard deviation (the radius), spatial pattern correlation coefficient (PCC) (cosine of the angle) and root-mean-square error (RMSE) (semicircle with a dashed/single-dotted line) from the RCM results are shown. In the figure, the closer the model result is to the Ref point (the blue dot), the better the model performance in the region. All individual model results show high spatial correlation coefficients above 0.75 for the entire CORDEX-EA Phase 2 domain (Figure 5a). The Rep_ENS and His_ENS show higher PCC and lower RMSE than other single models for reproduction and historical experiments, showing better performance. Rep_ENS presents substantial improvements over other individual RCMs of the reproduction experiments in all three monsoon regions. For His_ENS, the PCC is higher than the CMIP5 GCM_ENS but shows poorer performance from the RMSE perspective. However, in the ISM region, His_ENS is located closer to the Ref point than the CMIP5 GCM_ENS and most of the other individual models of historical experiments (Figure 5c). In the WNPSM region, the RCMs show relatively poor simulated performance, compared to other regions, with respect to the large bias in the ocean area (Figure 5d).

The above results demonstrate that an RCM ensemble can depict observation patterns better than other individual models. For this reason, only the ensemble results will be presented hereafter. Figure 6 presents the frequency of occurrence in summer based on the intensity of daily precipitation. Occurrence frequency is shown as a percentage, and events with no precipitation are excluded. ERA-Interim

shows that all three monsoon regions reveal a similar exponential pattern, and higher frequency appears in the ISM and WNPSM regions, compared to the EASM region for precipitation intensity greater than $200\text{ mm}\cdot\text{day}^{-1}$. In the model experiments, reasonable simulations appear for weak-intensity precipitation. Rep_ENS simulates distributions similar to the observation, especially in the EASM where precipitation below $60\text{ mm}\cdot\text{day}^{-1}$, but slightly overestimates precipitation at under $80\text{ mm}\cdot\text{day}^{-1}$ in the ISM and WNPSM regions. For high-intensity precipitation ($\geq 100\text{ mm}\cdot\text{day}^{-1}$), the Rep_ENS distribution is very close to observation, showing good performance. Also, the added value from His_ENS is shown in high-intensity precipitation. The CMIP5 GCM_ENS rarely shows frequency of occurrence at precipitation intensities of $100\text{ mm}\cdot\text{day}^{-1}$ or more. However, His_ENS shows an improved simulation ability for high-intensity precipitation in all regions. For low-intensity precipitation, both CMIP5 GCM_ENS and His_ENS show reasonable performance. Both results underestimate percentages in the EASM and ISM regions, while His_ENS presents a frequency higher than observation in the WNPSM region. The result of overestimating the frequency of low-intensity rainfall in the WNPSM region is related to wet bias in the western North Pacific, shown in Figure 4f.

Evaluating the simulated performance of the reproduction and historical experiments confirms that the RCM simulates the characteristics of summer precipitation in CORDEX-EA Phase 2 domain reasonably well. Using the RCM ensemble results, spatiotemporal

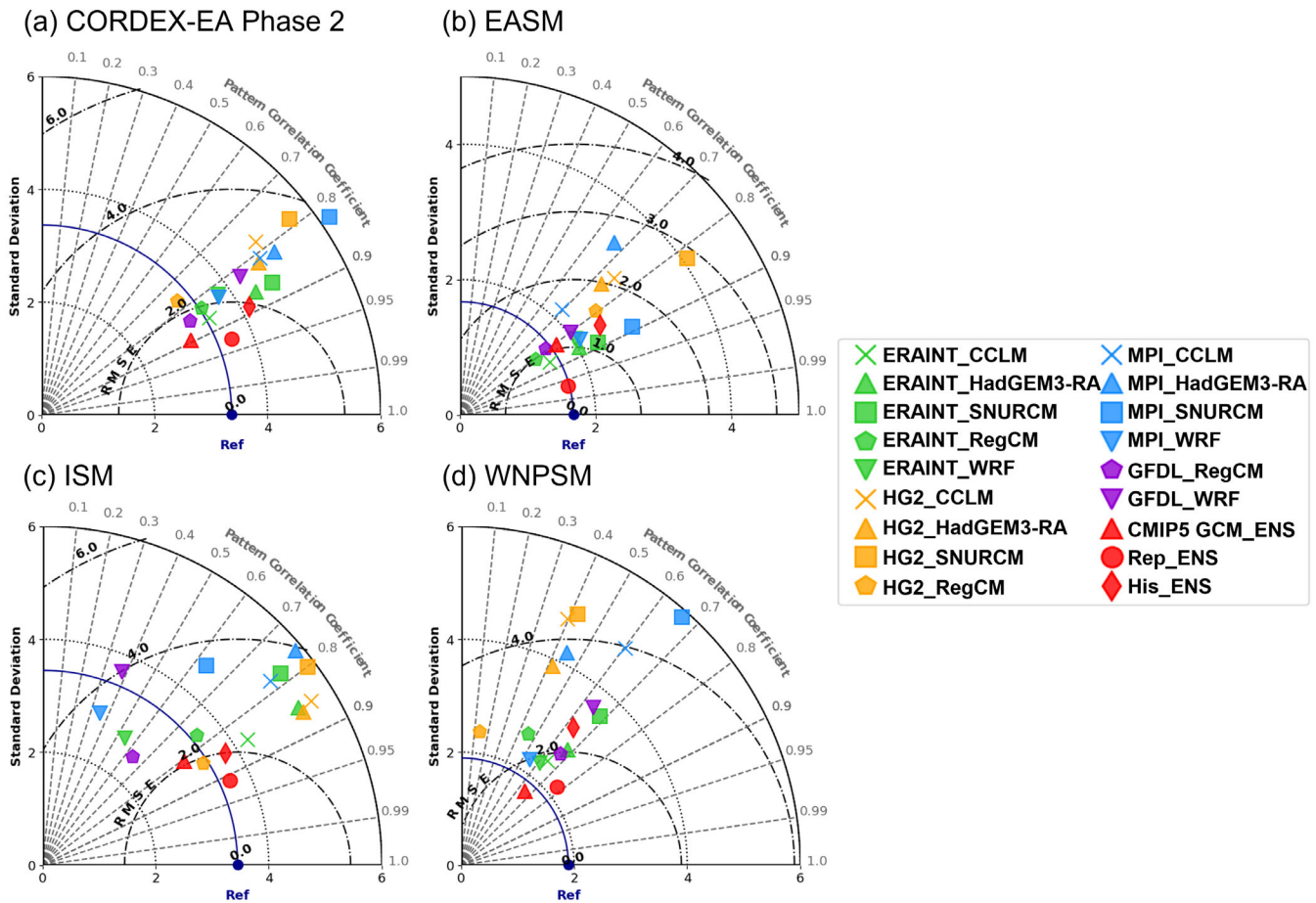


FIGURE 5 Taylor diagrams of summer (MJJAS) precipitation simulated by individual RCMs and model ensembles for the (a) CORDEX-East Asia Phase 2, (b) EASM, (c) ISM and (d) WNPSM region. Note that the scales differ between plots [Colour figure can be viewed at wileyonlinelibrary.com]

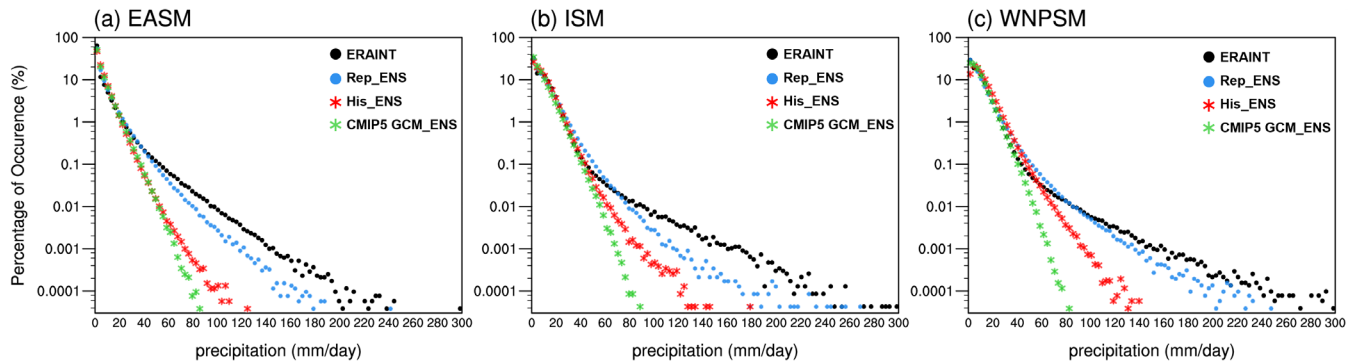


FIGURE 6 The percentages of occurrence for summer (MJJAS) daily precipitation derived from ERA-Interim, Rep_ENS, His_ENS, and the CMIP5 GCM ensemble for (a) EASM, (b) ISM and (c) WNPSM regions [Colour figure can be viewed at wileyonlinelibrary.com]

distributions of climate factors related to the ASM, such as precipitation and moisture flux, are analysed utilizing CSEOF. Although the ASM has different characteristics in each region, CSEOF is applied to the entire region of CORDEX-EA Phase 2 domain because of its connectivity between each region (Wang & Ho, 2002).

Figure 7 shows the first CSEOF mode of precipitation in CORDEX-EA Phase 2 domain derived from observation and each experiment. The first mode obviously represents the seasonal variation in precipitation (Lim et al., 2002), so the impact of typhoons would be almost neglected. The variance in ERA-Interim, Rep_ENS and His_ENS is

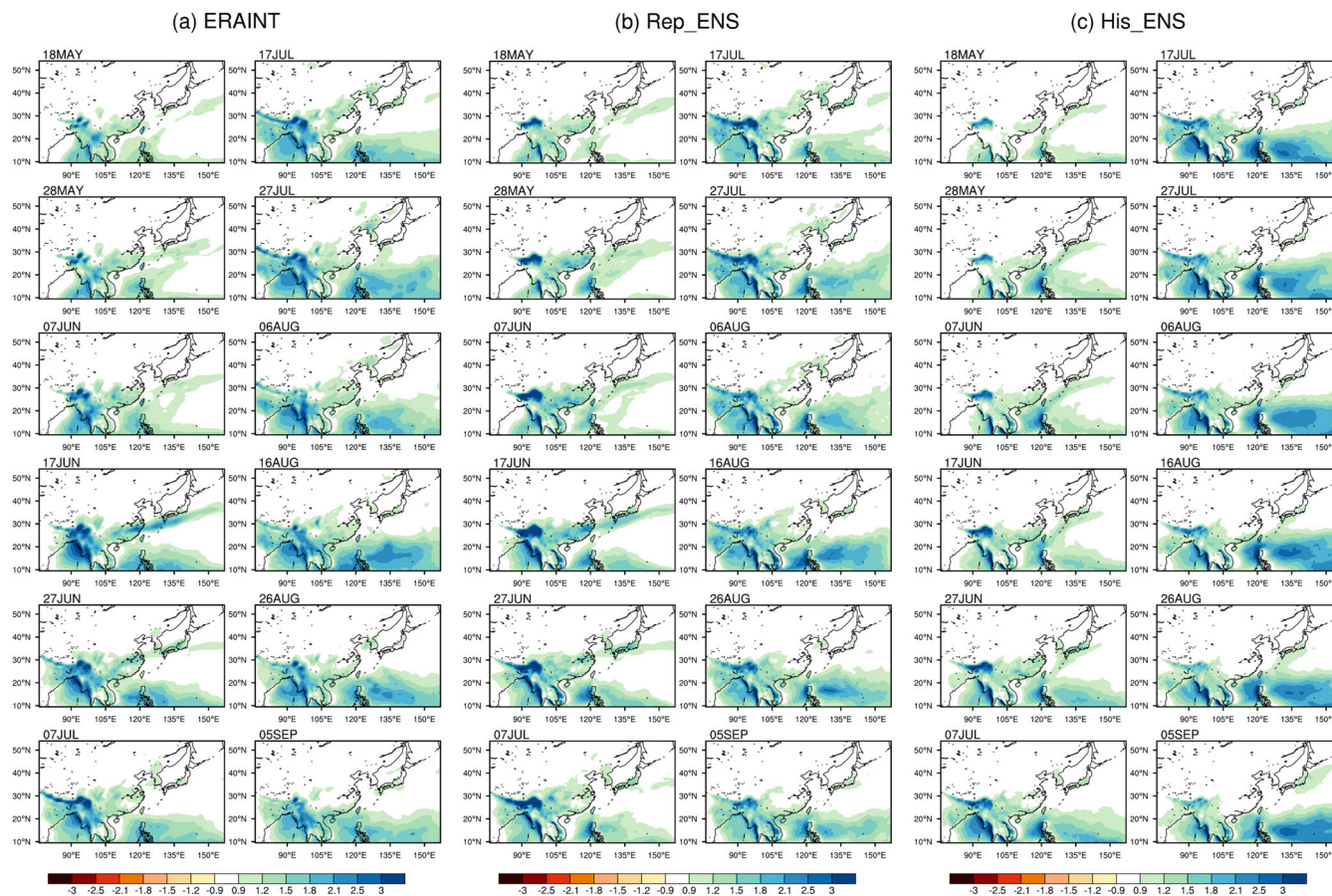


FIGURE 7 The first CSEOF mode of pentad mean precipitation over CORDEX-EA Phase 2 domain derived from (a) ERA-Interim, (b) Rep_ENS and (c) His_ENS. Left upper text of each figure denotes the date [Colour figure can be viewed at wileyonlinelibrary.com]

65.66%, 68.62% and 83.47%, respectively. In the first mode of observation, positive values increase in the eastern Bay of Bengal on 7 June and progress toward India (Figure 7a). Peak values appear in India on July, gradually weakening and disappearing after 16 August as the magnitude of precipitation decrease. This precipitation process in India is closely related to the eastward moisture flux at 850 hPa in India, which brings abundant moisture from the Indian Ocean (Li et al., 2012; Lim et al., 2002) (Figure S3a). Also, some of the eastward moisture flux moves to eastern China and Korea in July, which means that water transport from the ISM region may also affect the EASM. In the EASM region, a precipitation band passes through eastern China and below Japan near 30°N latitude on 17 June. As it moves north, positive precipitation appears in the EASM region during July. The precipitation band slowly vanishes and another large positive value appears over the western North Pacific after 6 August. In the WNPSM region, positive values increase after 17 July, reach a peak on 16 August, and after that it disappear.

In Rep_ENS, progression of the Indian summer monsoon is simulated well, although positive precipitation in the Bay of Bengal moving to the west is simulated as

being weaker than the observation, because of weakly simulated moisture flux vector (Figures 7b and S3b). Rep_ENS can capture the magnitude of precipitation and the time when the precipitation peak appears on the Indian Peninsula. The intensity of the precipitation band observed in the EASM region is underestimated, but its location and time of occurrence are depicted skilfully. Furthermore, in the WNPSM region, a positive peak appears around 16 August, indicating the summer monsoon period in the western Pacific is simulated well. His_ENS also represents well the westward propagation of precipitation over the Bay of Bengal during the same period, as observed (Figure 7c). His_ENS shows good performance in simulating precipitation from 18 May to 7 July in Bangladesh at an amount similar to observation. Propagating patterns of precipitation from 17 June to 27 July are well simulated over the Korean Peninsula and Japan, although the precipitation for the EASM region is depicted relatively weak. In regard to the underestimation, a cyclonic flow of moisture flux in His_ENS appears 6 August, about 10 days later than the observation, and its location appears further south (Figure S3). Supplement of water vapour to the Korean Peninsula and Japan

becomes low, resulting in less CSEOF mode 1 precipitation than the observation. For the WNPSM region, positive precipitation begins to increase significantly after 17 July, compared to observation, which seems to be due to the wet bias of summer mean precipitation in the region, as shown in Figure 4f. As precipitation in the WNPSM region gradually increases, a precipitation peak appears 16 August, consistent with the precipitation peak period in the WNPSM shown in the observation.

The performance for simulating characteristics of the precipitation band in the EASM region is analysed in detail. Figure 8 shows the latitude–time cross section for the first CSEOF mode of precipitation in the EASM region as averaged for 115°–135°E longitude. In ERA-Interim, precipitation of more than 1.5 begins to appear around 30°N and moves north in mid-June (Figure 8a). Propagating northward, three cores appear; the first is located near 30°N in mid-June, the second at 35°N in mid-July and the last at 42°N from the end of July to early August. Rep_ENS presents a very similar pattern to the observation (Figure 8b). In the three cores, the onset and process of monsoon rainfall are presented well.

His_ENS simulates generally less precipitation than observed, consistent with the results in Figure 4f (Figure 8c). In His_ENS, the time when precipitation moves northward appears around 30°N, about 5 days late, but the progress pattern is similar to that observed. The second core is not clearly shown, but the dissipation of precipitation in mid-July is simulated well at 35°N, where the Korean Peninsula is located. His_ENS also depicts well a migrating pattern in a precipitation band that moves northward up to 45°N and disappears gradually, similar to observation.

Figure 9 shows the second CSEOF mode of precipitation for each experiment. The variance in ERA-Interim, Rep_ENS and His_ENS, respectively, is 2.40%, 2.58% and 1.23%, showing much smaller values than the first mode. CSEOF mode 2 presents the intraseasonal variations in summer precipitation (Kim et al., 2019), with both positive and negative values, unlike mode 1. In the second CSEOF mode for ERA-Interim, strong variability is evident in the ocean region (Figure 9a). The positive and negative precipitation values stretch parallel to the zonal direction over the Korean Peninsula and Japan at the end

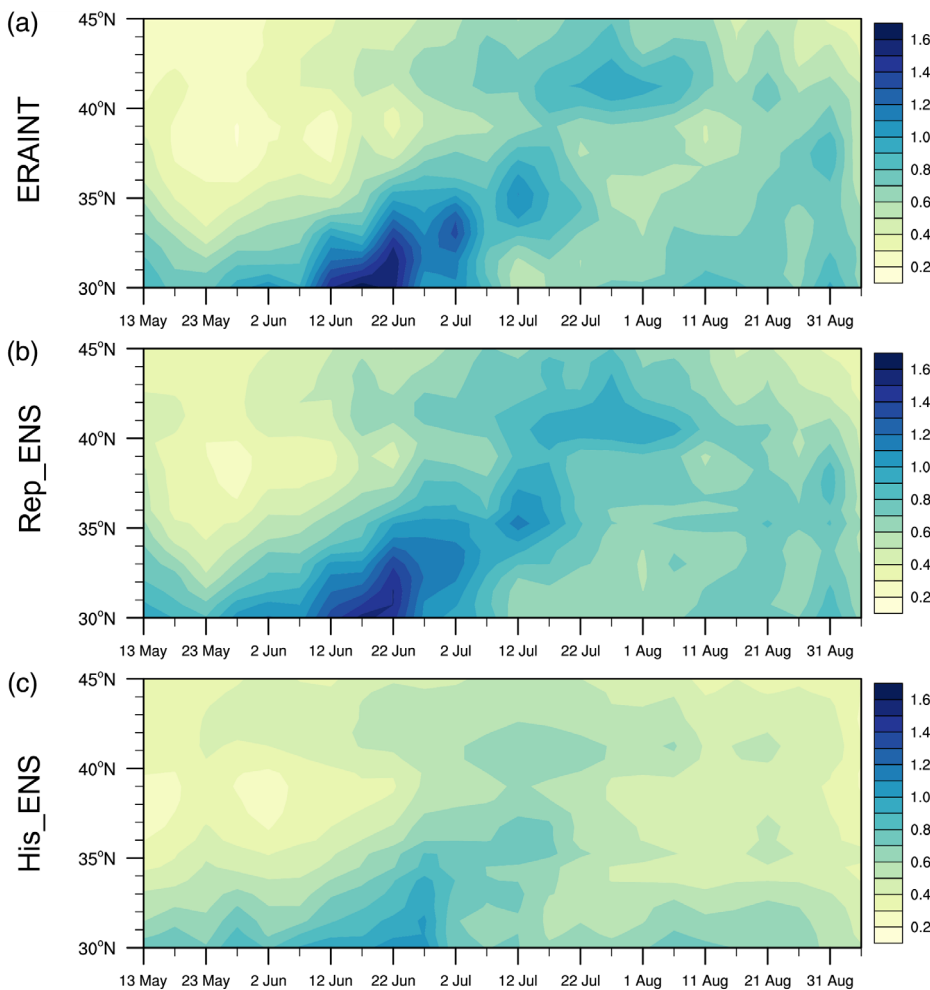


FIGURE 8 Latitude–time cross section diagrams of the first CSEOF mode of pentad mean precipitation averaged between 115°E and 135°E for (a) ERA-Interim, (b) Rep_ENS and (c) His_ENS [Colour figure can be viewed at wileyonlinelibrary.com]

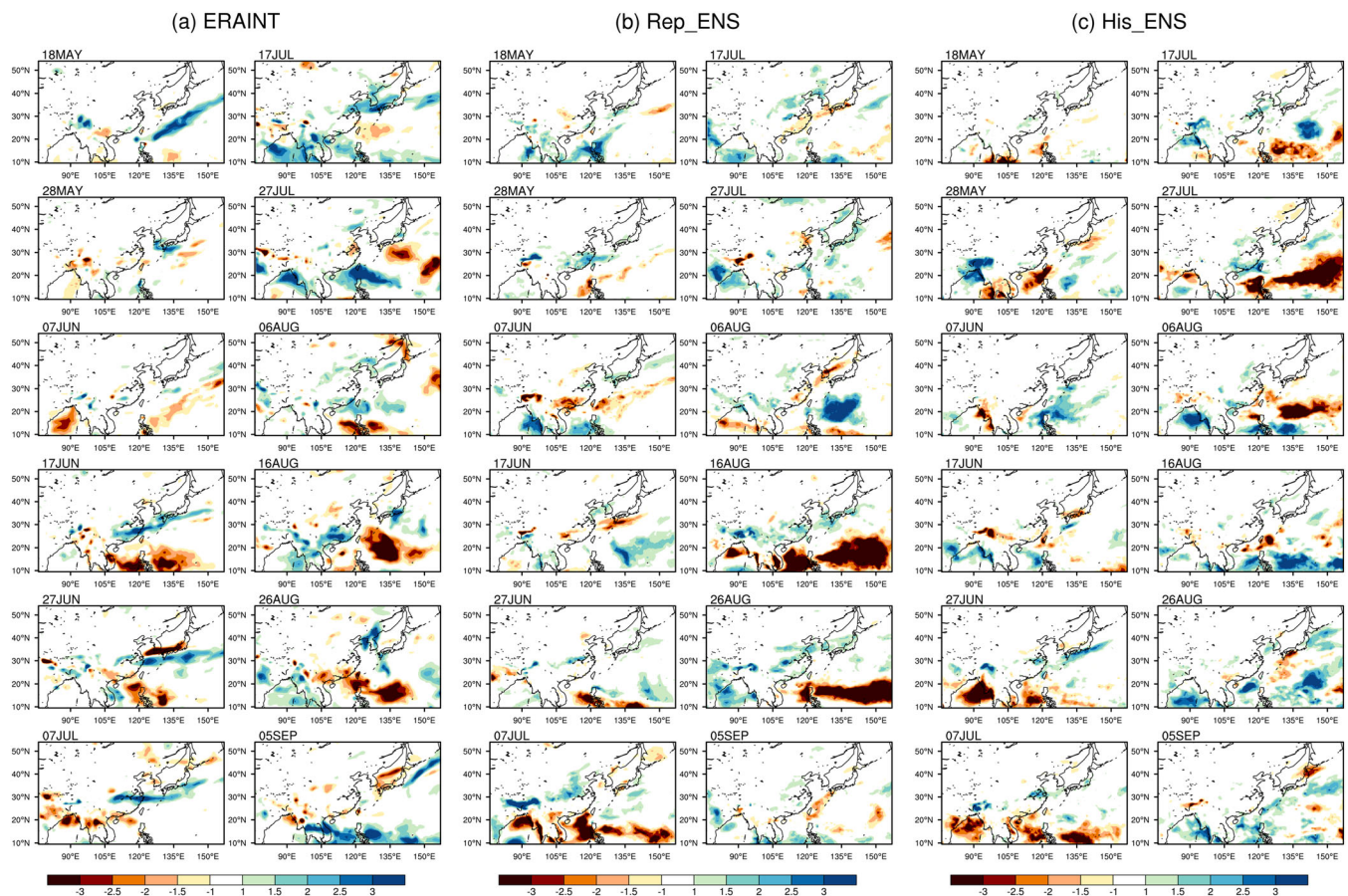


FIGURE 9 Same as Figure 7, but for the second CSEOF mode [Colour figure can be viewed at [wileyonlinelibrary.com](https://onlinelibrary.wiley.com/doi/10.1002/joc.8054)]

of June. The pattern is presented well in His_ENS, showing its capability to capture the intraseasonal variability of the EASM, whereas the simulation is slightly weak in Rep_ENS. The second major pattern in the observation is the negative precipitation value widely distributed in the WNPSM region on 16 August, which appears to be a break event in the western North Pacific summer monsoon (the WNPSM break) (Vega et al., 2020; Wang & Xu, 1997). Several studies argued that WNPSM breaks occur between the end of June and mid-July, and between mid-August and early September (Vega et al., 2020). Moreover, a composite of the precipitation anomalies in the inactive monsoon periods (i.e., WNPSM break days) shows negative precipitation anomalies in the WNPSM region, and Figure 9a also shows a clear negative value in the region from mid-August to the end of August, similar to a previous study. A strong anticyclonic moisture flux flow appears in that region, which is related to the WNPSM break in mid-August (Figure S4a). It is revealed that anticyclonic flow is detected at surface level over 10° – 28° N during the WNPSM break period by analysing NCEP-NCAR reanalysis data (Vega et al., 2020). Rep_ENS presents a negative value in the WNPSM region in the same

period as the observation (Figure 9b). However, it tends to overestimate the intensity of the WNPSM break, since the intensity of anticyclonic flow is simulated as stronger than the observation (Figure S4b). For His_ENS, the WNPSM break appears on 27 July, which is earlier than in the observation (Figure 9c). Also, the anticyclonic flow in His_ENS appears at that time with stronger intensity over a wider area than in the observation (Figure S4c).

4 | SUMMARY

The performance of multi-regional climate models simulating summer precipitation in CORDEX-EA Phase 2 domain is assessed by analysing the simulation results of RCMs forced by ERA-Interim reanalysis data (reproduction experiment) and CMIP5 GCM historical scenario data (historical experiment). RCM dynamical downscaling is conducted over the CORDEX-EA Phase 2 domain with a 25-km spatial resolution for the period from 1981 to 2005.

In general, the regional climate models well simulate the spatial patterns and frequency of occurrence for

summer (MJJAS) precipitation in CORDEX-EA Phase 2 domain. The spatial distribution of summer mean precipitation is depicted, to some extent, differently in each model, and generally shows systematic wet bias. Reproduction experiment simulates the spatial patterns in monsoon regions well, although more than half of the single RCMs overestimate precipitation on land. Meanwhile in the historical experiment, bias diminishes in Korean Peninsula and Indochina Peninsula, but wet bias exists over the western North Pacific compared to CMIP5 GCM_ENS. The RCM ensemble result for each experiment (Rep_ENS, His_ENS) represents a much smaller magnitude of bias than other individual RCMs, indicating superior performance in the ensemble results, compared to individual model results, for most of the regions. His_ENS can capture the characteristics of precipitation in complex terrain regions, which is not shown by the CMIP5 GCM_ENS, implying added value from the regional climate models. Furthermore, His_ENS shows less bias than the CMIP5 GCM for India, the Indochina Peninsula, and the Korean Peninsula. A performance index and Taylor diagram analysis (Figures 3 and 5) confirm that the ensemble results show remarkable performance, compared to the individual RCMs. Rep_ENS produces a better performance index for most of the regions compared to single RCMs of reproduction experiment. His_ENS shows a higher spatial correlation coefficient and a lower RMSE than other individual models in historical experiments for Asian precipitation. The frequency of occurrence, according to precipitation intensity, shows that the RCM ensembles tend to underestimate the frequency of strong precipitation at more than $60 \text{ mm}\cdot\text{day}^{-1}$. However, His_ENS simulates distributions of strong intensity precipitation that are much closer to the observation than the CMIP5 GCM, confirming added value from the RCM.

Cyclostationary EOF analysis revealed that the RCM ensembles describe spatiotemporal patterns of Asian precipitation that are similar to the observation. For the first CSEOF mode, which represents the seasonal variation of precipitation, both Rep_ENS and His_ENS show reasonable performance in simulating the evolution of the Asian summer monsoon. Peak period of precipitation from the Indian summer monsoon and the western North Pacific summer monsoon as well as the northward migration of the precipitation band in the East Asian summer monsoon are well represented. Compared to observation, His_ENS simulates cyclonic moisture flux later than the observation in early August, which is related to the underestimation of precipitation over the Korean Peninsula and Japan in mode 1. And the exaggerating the occurrence of weak precipitation that has a relatively high frequency of occurrence contributes to the overestimation of CSEOF mode 1 precipitation over the western North Pacific. Analysis is also

conducted on the precipitation characteristics of the precipitation band in EASM. Both Rep_ENS and His_ENS well capture the northward migration of the precipitation band in the EASM region, as well as the timing when the precipitation core appears. His_ENS underestimates the magnitude regarding to the lower supply of moisture than the observation. In the second CSEOF mode of precipitation, presenting intraseasonal variation, His_ENS describes two band-shaped precipitations with the opposite sign well, that appears in the EASM region at the end of June, similar to observation. Rep_ENS also captures the WNPSM break with the anticyclonic flow in late August, although His_ENS simulates it at about 10 days earlier than in the observation.

This study analysed the performance of regional climate models simulating the summer monsoons in the CORDEX-East Asia Phase 2 region in terms of temporal and spatial variations in precipitation. The results will be used for further precipitation studies using RCM simulations in the domain, including projections of precipitation in the future. One thing to note is that the models show relatively weak performance in the WNPSM region, compared to land areas, which may be due to a limitation in the RCM where it does not interactively simulate the air–sea interaction (Zou & Zhou, 2016). The monsoon in Asia is a phenomenon caused by land–sea contrast and sufficient moisture transport from the oceans, and thus the atmosphere–ocean interaction over the ocean is important (Lau & Li, 1984; Tao et al., 2016; Zhu et al., 2020). Therefore, it seems the model's performance regarding the monsoon can be determined by how well it simulates atmosphere–ocean interaction. Some studies (Samala et al., 2013; Wang et al., 2014; Zou & Zhou, 2016) argued that atmosphere–ocean-coupled regional climate models improve simulations of monsoon circulation and precipitation in Asia. However, the incomplete simulation of atmosphere–ocean flux exchanges in the coupled regional climate models causes climate drift as seen in the atmosphere–ocean coupled general circulation model, which eventually affects the model's capabilities for simulating model climate. Therefore, there is a certain limit to the model climate produced by the coupled regional model, and accordingly, the performance of the coupled climate model is still controversial.

AUTHOR CONTRIBUTIONS

Ga-Yeong Seo: Conceptualization; data curation; formal analysis; investigation; methodology; software; validation; visualization; writing – original draft; writing – review and editing. **Joong-Bae Ahn:** Conceptualization; methodology; project administration; supervision; validation; writing – review and editing. **Dong-Hyun Cha:** Data curation; project administration. **Myoung-Seok Suh:** Data curation; project administration. **Seung-Ki**

Min: Data curation; project administration. **Eun-Chul Chang:** Data curation; project administration. **Young-Hwa Byun:** Data curation; project administration. **Jin-Uk Kim:** Data curation; visualization.

ACKNOWLEDGEMENTS

This work was funded by the Korea Meteorological Administration Research and Development Program under Grant No. KMI2020-01411.

DATA AVAILABILITY STATEMENT

The model simulation data used in this study are available upon reasonable request from the authors, and will be publicly available at <https://esg-dn1.nsc.liu.se/search/cordex/> in the future. The ERA-Interim data can be downloaded at <https://apps.ecmwf.int/datasets/data/interim-full-daily/levtype=sfc>. The code for Cyclostationary EOF analysis is available at https://www2.cgd.ucar.edu/cas/software/SUBR_CYCLOSTATIONARY_WD.f90.html.

ORCID

Ga-Yeong Seo  <https://orcid.org/0000-0002-5119-1375>
 Joong-Bae Ahn  <https://orcid.org/0000-0001-6958-2801>
 Dong-Hyun Cha  <https://orcid.org/0000-0001-5053-6741>
 Myoung-Seok Suh  <https://orcid.org/0000-0002-3827-0044>
 Seung-Ki Min  <https://orcid.org/0000-0002-6749-010X>
 Eun-Chul Chang  <https://orcid.org/0000-0002-5784-447X>
 Young-Hwa Byun  <https://orcid.org/0000-0002-6074-4461>
 Jin-Uk Kim  <https://orcid.org/0000-0001-9892-9915>

REFERENCES

- Afrizal, T. & Surussavadee, C. (2018) High-resolution climate simulations in the Tropics with complex terrain employing the CESM/WRF model. *Advances in Meteorology*, 2018, 1–15. Available from: <https://doi.org/10.1155/2018/5707819>
- Annamalai, H. & Sperber, K.R. (2005) Regional heat sources and the active and break phases of boreal summer intraseasonal (30–50 day) variability. *Journal of the Atmospheric Sciences*, 62(8), 2726–2748. Available from: <https://doi.org/10.1175/jas3504.1>
- Ashfaq, M., Bowling, L.C., Cherkauer, K., Pal, J.S. & Diffenbaugh, N.S. (2010) Influence of climate model biases and daily-scale temperature and precipitation events on hydrological impacts assessment: A case study of the United States. *Journal of Geophysical Research: Atmospheres*, 115(D14), D14116. Available from: <https://doi.org/10.1029/2009jd012965>
- Ashfaq, M., Cavazos, T., Reboita, M.S., Torres-Alavez, J.A., Im, E.-S., Olusegun, C.F. et al. (2020) Robust late twenty-first century shift in the regional monsoons in RegCM-CORDEX simulations. *Climate Dynamics*, 57, 1463–1488. Available from: <https://doi.org/10.1007/s00382-020-05306-2>
- Baek, H.-J., Lee, J., Lee, H.-S., Hyun, Y.-K., Cho, C., Kwon, W.-T. et al. (2013) Climate change in the 21st century simulated by HadGEM2-AO under representative concentration pathways. *Asia-Pacific Journal of Atmospheric Sciences*, 49(5), 603–618. Available from: <https://doi.org/10.1007/s13143-013-0053-7>
- Bartók, B., Wild, M., Folini, D., Lüthi, D., Kotlarski, S., Schär, C. et al. (2017) Projected changes in surface solar radiation in CMIP5 global climate models and in EURO-CORDEX regional climate models for Europe. *Climate Dynamics*, 49(7), 2665–2683. Available from: <https://doi.org/10.1007/s00382-016-3471-2>
- Berg, P., Christensen, O., Klehmet, K., Lenderink, G., Olsson, J., Teichmann, C. et al. (2019) Summertime precipitation extremes in a EURO-CORDEX 0.11° ensemble at an hourly resolution. *Natural Hazards and Earth System Sciences*, 19, 957–971. Available from: <https://doi.org/10.5194/nhess-19-957-2019>
- Bergant, K., Belda, M. & Halenka, T. (2007) Systematic errors in the simulation of European climate (1961–2000) with RegCM3 driven by NCEP/NCAR reanalysis. *International Journal of Climatology*, 27(4), 455–472. Available from: <https://doi.org/10.1002/joc.1413>
- Best, M.J., Pryor, M., Clark, D.B., Rooney, G.G., Essery, R.L.H., Ménard, C.B. et al. (2011) The Joint UK Land Environment Simulator (JULES), model description—part 1: energy and water fluxes. *Geoscientific Model Development*, 4(3), 677–699. Available from: <https://doi.org/10.5194/gmd-4-677-2011>
- Betts, A.K. & Miller, M.J. (1986) A new convective adjustment scheme. Part II: single column tests using GATE wave, BOMEX, ATEX and arctic air-mass data sets. *Quarterly Journal of the Royal Meteorological Society*, 112(473), 693–709. Available from: <https://doi.org/10.1002/qj.49711247308>
- Bhaskaran, B., Jones, R.G., Murphy, J.M. & Noguer, M. (1996) Simulations of the Indian summer monsoon using a nested regional climate model: domain size experiments. *Climate Dynamics*, 12(9), 573–587. Available from: <https://doi.org/10.1007/BF00216267>
- Bonan, G.B., Oleson, K.W., Vertenstein, M., Levis, S., Zeng, X., Dai, Y. et al. (2002) The land surface climatology of the Community Land Model coupled to the NCAR Community Climate Model. *Journal of Climate*, 15(22), 3123–3149. Available from: [https://doi.org/10.1175/1520-0442\(2002\)015<3123:Tlscot>2.0.Co;2](https://doi.org/10.1175/1520-0442(2002)015<3123:Tlscot>2.0.Co;2)
- Briegleb, B.P. (1992) Delta-Eddington approximation for solar radiation in the NCAR community climate model. *Journal of Geophysical Research*, 97, 7603. Available from: <https://doi.org/10.1029/92jd00291>
- Cash, B.A., Kinter, J.L., Adams, J., Altshuler, E., Huang, B., Jin, E. K. et al. (2015) Regional structure of the Indian summer monsoon in observations, reanalysis, and simulation. *Journal of Climate*, 28(5), 1824–1841. Available from: <https://doi.org/10.1175/jcli-d-14-00292.1>
- Chang, C.-P., Zhang, Y. & Li, T. (2000) Interannual and interdecadal variations of the East Asian summer monsoon and tropical Pacific SSTs. Part I: roles of the subtropical ridge. *Journal of Climate*, 13(24), 4310–4325.
- Chen, F. & Dudhia, J. (2001) Coupling an Advanced Land Surface–Hydrology Model with the Penn State–NCAR MM5 modeling system. Part I: model implementation and sensitivity. *Monthly Weather Review*, 129(4), 569–585. Available from: [https://doi.org/10.1175/1520-0493\(2001\)129<0569:Caalsh>2.0.Co;2](https://doi.org/10.1175/1520-0493(2001)129<0569:Caalsh>2.0.Co;2)

- Chu, J.-E., Hameed, S.N. & Ha, K.-J. (2012) Nonlinear, intraseasonal phases of the East Asian summer monsoon: extraction and analysis using self-organizing maps. *Journal of Climate*, 25(20), 6975–6988. Available from: <https://doi.org/10.1175/jcli-d-11-00512.1>
- Collins, W.D., Hackney, J.K. & Edwards, D.P. (2002) An updated parameterization for infrared emission and absorption by water vapor in the National Center for Atmospheric Research Community Atmosphere Model. *Journal of Geophysical Research*, 107(D22), 4664. Available from: <https://doi.org/10.1029/2001jd001365>
- Cusack, S., Edwards, J.M. & Crowther, J.M. (1999) Investigating k distribution methods for parameterizing gaseous absorption in the Hadley Centre Climate Model. *Journal of Geophysical Research: Atmospheres*, 104(D2), 2051–2057. Available from: <https://doi.org/10.1029/1998JD200063>
- da Rocha, R.P., Morales, C.A., Cuadra, S.V. & Ambrizzi, T. (2009) Precipitation diurnal cycle and summer climatology assessment over South America: an evaluation of Regional Climate Model version 3 simulations. *Journal of Geophysical Research: Atmospheres*, 114(D10), D10108. Available from: <https://doi.org/10.1029/2008jd010212>
- Dash, S.K., Kulkarni, M.A., Mohanty, U.C. & Prasad, K. (2009) Changes in the characteristics of rain events in India. *Journal of Geophysical Research: Atmospheres*, 114(D10), D10109. Available from: <https://doi.org/10.1029/2008JD010572>
- Dash, S.K., Shekhar, M.S. & Singh, G.P. (2006) Simulation of Indian summer monsoon circulation and rainfall using RegCM3. *Theoretical and Applied Climatology*, 86(1), 161–172. Available from: <https://doi.org/10.1007/s00704-006-0204-1>
- Déqué, M., Rowell, D.P., Lüthi, D., Giorgi, F., Christensen, J.H., Rockel, B. et al. (2007) An intercomparison of regional climate simulations for Europe: assessing uncertainties in model projections. *Climatic Change*, 81, 53–70. Available from: <https://doi.org/10.1007/s10584-006-9228-x>
- Diallo, I., Sylla, M.B., Giorgi, F., Gaye, A.T. & Camara, M. (2012) Multimodel GCM-RCM ensemble-based projections of temperature and precipitation over West Africa for the early 21st century. *International Journal of Geophysics*, 2012, 972896. Available from: <https://doi.org/10.1155/2012/972896>
- Ding, Q. & Wang, B. (2007) Intraseasonal teleconnection between the summer Eurasian wave train and the Indian monsoon. *Journal of Climate*, 20(15), 3751–3767. Available from: <https://doi.org/10.1175/jcli4221.1>
- Ding, Y. (2007) The variability of the Asian summer monsoon. *Journal of the Meteorological Society of Japan Ser. II*, 85, 21–54. Available from: <https://doi.org/10.2151/jmsj.85B.21>
- Dosio, A. (2016) Projections of climate change indices of temperature and precipitation from an ensemble of bias-adjusted high-resolution EURO-CORDEX regional climate models. *Journal of Geophysical Research: Atmospheres*, 121(10), 5488–5511. Available from: <https://doi.org/10.1002/2015jd024411>
- Dunne, J.P., John, J.G., Adcroft, A.J., Griffies, S.M., Hallberg, R.W., Shevliakova, E. et al. (2012) GFDL's ESM2 Global Coupled Climate–Carbon Earth System models. Part I: physical formulation and baseline simulation characteristics. *Journal of Climate*, 25(19), 6646–6665. Available from: <https://doi.org/10.1175/jcli-d-11-00560.1>
- Edwards, J.M. & Slingo, A. (1996) Studies with a flexible new radiation code. I: choosing a configuration for a large-scale model. *Quarterly Journal of the Royal Meteorological Society*, 122(531), 689–719. Available from: <https://doi.org/10.1002/qj.49712253107>
- Emanuel, K.A. (1991) A scheme for representing cumulus convection in large-scale models. *Journal of Atmospheric Sciences*, 48(21), 2313–2329. Available from: [https://doi.org/10.1175/1520-0469\(1991\)048<2313:Asfrec>2.0.Co;2](https://doi.org/10.1175/1520-0469(1991)048<2313:Asfrec>2.0.Co;2)
- Fantini, A., Raffaele, F., Torma, C., Bacer, S., Coppola, E., Giorgi, F. et al. (2018) Assessment of multiple daily precipitation statistics in ERA-Interim driven Med-CORDEX and EURO-CORDEX experiments against high resolution observations. *Climate Dynamics*, 51(3), 877–900. Available from: <https://doi.org/10.1007/s00382-016-3453-4>
- Feser, F., Rockel, B., von Storch, H., Winterfeldt, J. & Zahn, M. (2011) Regional climate models add value to global model data: a review and selected examples. *Bulletin of the American Meteorological Society*, 92(9), 1181–1192. Available from: <https://doi.org/10.1175/2011bams3061.1>
- Fu, C. & Zeng, Z. (1997) Monsoon regions: the areas with the largest precipitation variability in the world. *Chinese Science Bulletin*, 42(21), 2306–2309.
- Gao, X., Shi, Y., Song, R., Giorgi, F., Wang, Y. & Zhang, D. (2008) Reduction of future monsoon precipitation over China: comparison between a high resolution RCM simulation and the driving GCM. *Meteorology and Atmospheric Physics*, 100(1–4), 73–86. Available from: <https://doi.org/10.1007/s00703-008-0296-5>
- Gelaro, R., McCarty, W., Suárez, M.J., Todling, R., Molod, A., Takacs, L. et al. (2017) The Modern-Era retrospective analysis for research and applications, version 2 (MERRA-2). *Journal of Climate*, 30(14), 5419–5454. Available from: <https://doi.org/10.1175/jcli-d-16-0758.1>
- Giorgetta, M.A., Jungclaus, J., Reick, C.H., Legutke, S., Bader, J., Böttinger, M. et al. (2013) Climate and carbon cycle changes from 1850 to 2100 in MPI-ESM simulations for the Coupled Model Intercomparison Project Phase 5. *Journal of Advances in Modeling Earth Systems*, 5(3), 572–597. Available from: <https://doi.org/10.1002/jame.20038>
- Giorgi, F. (2006) Regional climate modeling: status and perspectives. *Journal de Physique IV France*, 139, 101–118. Available from: <https://doi.org/10.1051/jp4:2006139008>
- Grant, A. & Brown, A.R. (1999) A similarity hypothesis for shallow cumulus transports. *Quarterly Journal of the Royal Meteorological Society*, 125(558), 1913–1936. Available from: <https://doi.org/10.1002/QJ.49712555802>
- Gregory, D. & Rowntree, P.R. (1990) A mass flux convection scheme with representation of cloud ensemble characteristics and stability-dependent closure. *Monthly Weather Review*, 118(7), 1483–1506. Available from: [https://doi.org/10.1175/1520-0493\(1990\)118<1483:Amfcsw>2.0.Co;2](https://doi.org/10.1175/1520-0493(1990)118<1483:Amfcsw>2.0.Co;2)
- Gu, H., Yu, Z., Yang, C., Ju, Q., Yang, T. & Zhang, D. (2018) High-resolution ensemble projections and uncertainty assessment of regional climate change over China in CORDEX East Asia. *Hydrology and Earth System Sciences*, 22(5), 3087–3103. Available from: <https://doi.org/10.5194/hess-22-3087-2018>
- Ha, K.-J., Heo, K.-Y., Lee, S.-S., Yun, K.-S. & Jhun, J.-G. (2012) Variability in the East Asian monsoon: a review. *Meteorological Applications*, 19(2), 200–215. Available from: <https://doi.org/10.1002/met.1320>
- Hamlington, B.D., Leben, R.R. & Kim, K.Y. (2012) Improving sea level reconstructions using non-sea level measurements.

- Journal of Geophysical Research: Oceans*, 117(C10), C10025. Available from: <https://doi.org/10.1029/2012jc008277>
- Hamlington, B.D., Leben, R.R., Strassburg, M.W. & Kim, K.-Y. (2014) Cyclostationary empirical orthogonal function sea-level reconstruction. *Geoscience Data Journal*, 1(1), 13–19. Available from: <https://doi.org/10.1002/gdj3.6>
- Harris, I., Jones, P.D., Osborn, T.J. & Lister, D.H. (2014) Updated high-resolution grids of monthly climatic observations—the CRU TS3.10 dataset. *International Journal of Climatology*, 34(3), 623–642. Available from: <https://doi.org/10.1002/joc.3711>
- Herrera, S., Fita, L., Fernández, J. & Gutiérrez, J.M. (2010) Evaluation of the mean and extreme precipitation regimes from the ENSEMBLES regional climate multimodel simulations over Spain. *Journal of Geophysical Research: Atmospheres*, 115(D21), D21117. Available from: <https://doi.org/10.1029/2010JD013936>
- Hong, J.-Y. & Ahn, J.-B. (2015) Changes of early summer precipitation in the Korean peninsula and nearby regions based on RCP simulations. *Journal of Climate*, 28(9), 3557–3578. Available from: <https://doi.org/10.1175/jcli-d-14-00504.1>
- Hong, S.-Y., Dudhia, J. & Chen, S.-H. (2004) A revised approach to ice microphysical processes for the bulk parameterization of clouds and precipitation. *Monthly Weather Review*, 132(1), 103–120. Available from: [https://doi.org/10.1175/1520-0493\(2004\)132<0103:Aratim>2.0.Co;2](https://doi.org/10.1175/1520-0493(2004)132<0103:Aratim>2.0.Co;2)
- Hong, S.-Y. & Kanamitsu, M. (2014) Dynamical downscaling: fundamental issues from an NWP point of view and recommendations. *Asia-Pacific Journal of Atmospheric Sciences*, 50(1), 83–104. Available from: <https://doi.org/10.1007/s13143-014-0029-2>
- Hrudya, P.H., Varikoden, H. & Vishnu, R. (2020) A review on the Indian summer monsoon rainfall, variability and its association with ENSO and IOD. *Meteorology and Atmospheric Physics*, 133(1), 1–14. Available from: <https://doi.org/10.1007/s00703-020-00734-5>
- Huang, B., Polanski, S. & Cubasch, U. (2015) Assessment of precipitation climatology in an ensemble of CORDEX-East Asia regional climate simulations. *Climate Research*, 64(2), 141–158. Available from: <https://doi.org/10.3354/cr01302>
- Huth, R., Kyselý, J. & Pokorná, L. (2000) A GCM simulation of heat waves, dry spells, and their relationships to circulation. *Climatic Change*, 46(1), 29–60. Available from: <https://doi.org/10.1023/A:1005633925903>
- Im, E.-S., Choi, Y.-W. & Ahn, J.-B. (2016) Robust intensification of hydroclimatic intensity over East Asia from multi-model ensemble regional projections. *Theoretical and Applied Climatology*, 129(3–4), 1241–1254. Available from: <https://doi.org/10.1007/s00704-016-1846-2>
- Im, E.-S., Kwon, W.-T., Ahn, J.-B. & Giorgi, F. (2007) Multi-decadal scenario simulation over Korea using a one-way double-nested regional climate model system. Part 1: recent climate simulation (1971–2000). *Climate Dynamics*, 28(7), 759–780. Available from: <https://doi.org/10.1007/s00382-006-0203-z>
- IPCC. (2013) *Climate change 2013: the physical science basis. Contribution of working group I to the fifth assessment report of the intergovernmental panel on climate change*. Cambridge and New York, NY: Cambridge University Press.
- Janes, T., McGrath, F., Macadam, I. & Jones, R. (2019) High-resolution climate projections for South Asia to inform climate impacts and adaptation studies in the Ganges-Brahmaputra-Meghna and Mahanadi deltas. *Science of the Total Environment*, 650, 1499–1520. Available from: <https://doi.org/10.1016/j.scitotenv.2018.08.376>
- Janjić, Z.I. (1994) The Step-Mountain eta coordinate model: further developments of the convection, viscous sublayer, and turbulence closure schemes. *Monthly Weather Review*, 122(5), 927–945. Available from: [https://doi.org/10.1175/1520-0493\(1994\)122<0927:Tsmecm>2.0.Co;2](https://doi.org/10.1175/1520-0493(1994)122<0927:Tsmecm>2.0.Co;2)
- Jin, C.-S., Cha, D.-H., Lee, D.-K., Suh, M.-S., Hong, S.-Y., Kang, H.-S. et al. (2016) Evaluation of climatological tropical cyclone activity over the western North Pacific in the CORDEX-East Asia multi-RCM simulations. *Climate Dynamics*, 47(3), 765–778. Available from: <https://doi.org/10.1007/s00382-015-2869-6>
- Jo, S., J.-B. Ahn, D.-h. Cha, S.-K. Min, M.-S. Suh, Y.-H. Byun, and J.-U. Kim. (2019) The Köppen–Trewartha climate-type changes over the CORDEX-East Asia Phase 2 domain under 2 and 3°C global warming. *Geophysical Research Letters*, 46(23), 14030–14041. doi:<https://doi.org/10.1029/2019GL085452>
- Kain, J.S. (2004) The Kain–Fritsch convective parameterization: an update. *Journal of Applied Meteorology*, 43(1), 170–181. Available from: [https://doi.org/10.1175/1520-0450\(2004\)043<0170:Tkepau>2.0.Co;2](https://doi.org/10.1175/1520-0450(2004)043<0170:Tkepau>2.0.Co;2)
- Kang, H.-S. & Hong, S.-Y. (2008) Sensitivity of the simulated East Asian summer monsoon climatology to four convective parameterization schemes. *Journal of Geophysical Research: Atmospheres*, 113(D15), D15119. Available from: <https://doi.org/10.1029/2007jd009692>
- Karmacharya, J., Jones, R., Moufouma-Okia, W. & New, M. (2017) Evaluation of the added value of a high-resolution regional climate model simulation of the South Asian summer monsoon climatology. *International Journal of Climatology*, 37(9), 3630–3643. Available from: <https://doi.org/10.1002/joc.4944>
- Kiehl, J., Hack, J., Bonan, G., Boville, B., Briegleb, B., Williamson, D. et al. (1996) *Description of the NCAR community climate model (CCM3)*. Boulder, CO: NCAR. NCAR technical note NCAR/TN-420+STR.
- Kim, G., Cha, D.-H., Park, C., Jin, C.-S., Lee, D.-K., Suh, M.-S. et al. (2021) Evaluation and projection of regional climate over East Asia in CORDEX-East Asia Phase I experiment. *Asia-Pacific Journal of Atmospheric Sciences*, 57(1), 119–134. Available from: <https://doi.org/10.1007/s13143-020-00180-8>
- Kim, K.-Y., Kim, J., Boo, K.-O., Shim, S. & Kim, Y. (2019) Intercomparison of precipitation datasets for summer precipitation characteristics over East Asia. *Climate Dynamics*, 52(5–6), 3005–3022. Available from: <https://doi.org/10.1007/s00382-018-4303-3>
- Kim, K.Y. & Kim, Y.Y. (2004) Investigation of tropical Pacific upper-ocean variability using cyclostationary EOFs of assimilated data. *Ocean Dynamics*, 54(5), 489–505. Available from: <https://doi.org/10.1007/s10236-004-0094-7>
- Kim, K.-Y., Lim, C.-Y. & Kim, E.J. (2018) A new approach to the space–time analysis of big data: application to subway traffic data in Seoul. *Journal of Big Data*, 5(1), 5. Available from: <https://doi.org/10.1186/s40537-018-0116-9>
- Kim, K.-Y. & North, G.R. (1997) EOFs of harmonizable cyclostationary processes. *Journal of the Atmospheric Sciences*, 54(19), 2416–2427. Available from: [https://doi.org/10.1175/1520-0469\(1997\)054<2416:EOhpc>2.0.Co;2](https://doi.org/10.1175/1520-0469(1997)054<2416:EOhpc>2.0.Co;2)
- Kim, K.-Y., North, G.R. & Huang, J. (1996) EOFs of one-dimensional cyclostationary time series: computations, examples, and

- stochastic modeling. *Journal of the Atmospheric Sciences*, 53(7), 1007–1017. Available from: [https://doi.org/10.1175/1520-0469\(1996\)053<1007:eoodct>2.0.co;2](https://doi.org/10.1175/1520-0469(1996)053<1007:eoodct>2.0.co;2)
- Kwon, M., Jhun, J.-G., Wang, B., An, S.-I. & Kug, J.-S. (2005) Decadal change in relationship between East Asian and WNP summer monsoons. *Geophysical Research Letters*, 32(16), L16709. Available from: <https://doi.org/10.1029/2005GL023026>
- Lau, K.-M. & Li, M.-T. (1984) The monsoon of East Asia and its global associations—a survey. *Bulletin of the American Meteorological Society*, 65(2), 114–125. Available from: [https://doi.org/10.1175/1520-0477\(1984\)065<0114:Tmoeaa>2.0.Co;2](https://doi.org/10.1175/1520-0477(1984)065<0114:Tmoeaa>2.0.Co;2)
- Lee, D.-K. & Suh, M.-S. (2000) Ten-year East Asian summer monsoon simulation using a regional climate model (RegCM2). *Journal of Geophysical Research: Atmospheres*, 105(D24), 29565–29577. Available from: <https://doi.org/10.1029/2000JD900438>
- Lee, H., Jin, C.-S., Cha, D.-H., Lee, M., Lee, D.-K., Suh, M.-S. et al. (2019) Future change in tropical cyclone activity over the Western North Pacific in CORDEX-East Asia multi-RCMs forced by HadGEM2-AO. *Journal of Climate*, 32(16), 5053–5067. Available from: <https://doi.org/10.1175/jcli-d-18-0575.1>
- Lee, M., Cha, D.-H., Suh, M.-S., Chang, E.-C., Ahn, J.-B., Min, S.-K. et al. (2020) Comparison of tropical cyclone activities over the western North Pacific in CORDEX-East Asia Phase I and II experiments. *Journal of Climate*, 33(24), 10593–10607. Available from: <https://doi.org/10.1175/jcli-d-19-1014.1>
- Lee, S.-S., Seo, Y.-W., Ha, K.-J. & Jhun, J.-G. (2013) Impact of the western North Pacific subtropical high on the East Asian monsoon precipitation and the Indian Ocean precipitation in the boreal summertime. *Asia-Pacific Journal of Atmospheric Sciences*, 49(2), 171–182. Available from: <https://doi.org/10.1007/s13143-013-0018-x>
- Li, D., Yin, B., Feng, J., Dosio, A., Geyer, B., Qi, J. et al. (2018a) Present climate evaluation and added value analysis of dynamically downscaled simulations of CORDEX-East Asia. *Journal of Applied Meteorology and Climatology*, 57(10), 2317–2341. Available from: <https://doi.org/10.1175/jamc-d-18-0008.1>
- Li, H., Chen, H., Wang, H. & Yu, E. (2018b) Future precipitation changes over China under 1.5°C and 2.0°C global warming targets by using CORDEX regional climate models. *Science of the Total Environment*, 640–641, 543–554. Available from: <https://doi.org/10.1016/j.scitotenv.2018.05.324>
- Li, T. & Wang, B. (2005) A review on the western North Pacific monsoon: synoptic-to-interannual variabilities. *Terrestrial Atmospheric and Oceanic Sciences*, 16, 285–314. Available from: [https://doi.org/10.3319/TAO.2005.16.2.285\(A\)](https://doi.org/10.3319/TAO.2005.16.2.285(A))
- Li, W., Guo, W., Xue, Y., Fu, C. & Qiu, B. (2016) Sensitivity of a regional climate model to land surface parameterization schemes for East Asian summer monsoon simulation. *Climate Dynamics*, 47(7), 2293–2308. Available from: <https://doi.org/10.1007/s00382-015-2964-8>
- Li, X., Wen, Z., Zhou, W. & Wang, D. (2012) Atmospheric water vapor transport associated with two decadal rainfall shifts over east China. *Journal of the Meteorological Society of Japan. Ser. II*, 90(5), 587–602. Available from: <https://doi.org/10.2151/jmsj.2012-501>
- Li, Z., Sun, Y., Li, T., Ding, Y. & Hu, T. (2019) Future changes in East Asian summer monsoon circulation and precipitation under 1.5 to 5°C of warming. *Earth's Futures*, 7(12), 1391–1406. Available from: <https://doi.org/10.1029/2019ef001276>
- Lim, Y.-K. & Kim, K.-Y. (2007) ENSO impact on the space–time evolution of the regional Asian summer monsoons. *Journal of Climate*, 20(11), 2397–2415. Available from: <https://doi.org/10.1175/jcli4120.1>
- Lim, Y.-K., Kim, K.-Y. & Lee, H.-S. (2002) Temporal and spatial evolution of the Asian summer monsoon in the seasonal cycle of synoptic fields. *Journal of Climate*, 15(24), 3630–3644. Available from: [https://doi.org/10.1175/1520-0442\(2002\)015<3630:Taseot>2.0.Co;2](https://doi.org/10.1175/1520-0442(2002)015<3630:Taseot>2.0.Co;2)
- Liu, B., Liu, Y., Wu, G., Yan, J., He, J. & Ren, S. (2015) Asian summer monsoon onset barrier and its formation mechanism. *Climate Dynamics*, 45(3), 711–726. Available from: <https://doi.org/10.1007/s00382-014-2296-0>
- Liu, Y., Giorgi, F. & Washington, W.M. (1994) Simulation of summer monsoon climate over East Asia with an NCAR regional climate model. *Monthly Weather Review*, 122(10), 2331–2348. Available from: [https://doi.org/10.1175/1520-0493\(1994\)122<2331:Sosmco>2.0.Co;2](https://doi.org/10.1175/1520-0493(1994)122<2331:Sosmco>2.0.Co;2)
- Loève, M. (1978) *Probability theory II*, 4th edition. New York, NY: Springer.
- Lu, R. (2001) Interannual variability of the summertime North Pacific subtropical high and its relation to atmospheric convection over the Warm Pool. *Journal of the Meteorological Society of Japan. Ser. II*, 79(3), 771–783. Available from: <https://doi.org/10.2151/jmsj.79.771>
- Mariotti, L., Diallo, I., Coppola, E. & Giorgi, F. (2014) Seasonal and intraseasonal changes of African monsoon climates in 21st century CORDEX projections. *Climatic Change*, 125(1), 53–65. Available from: <https://doi.org/10.1007/s10584-014-1097-0>
- Marsh, P.T., Brooks, H.E. & Karoly, D.J. (2007) Assessment of the severe weather environment in North America simulated by a global climate model. *Atmospheric Science Letters*, 8(4), 100–106. Available from: <https://doi.org/10.1002/asl.159>
- Merino, A., García-Ortega, E., Navarro, A., Fernández-González, S., Tapiador, F.J. & Sánchez, J.L. (2021) Evaluation of gridded rain-gauge-based precipitation datasets: impact of station density, spatial resolution, altitude gradient and climate. *International Journal of Climatology*, 41(5), 3027–3043. Available from: <https://doi.org/10.1002/joc.7003>
- Murakami, T. & Matsumoto, J. (1994) Summer monsoon over the Asian continent and western North Pacific. *Journal of the Meteorological Society of Japan. Ser. II*, 72(5), 719–745. Available from: https://doi.org/10.2151/jmsj1965.72.5_719
- Noh, T.G., Yeh, S.W., Hyun, Y.K. & Hwang, S.O. (2020) Non-stationary characteristics of intraseasonal precipitation variability in Northeast Asia during the boreal summer. *International Journal of Climatology*, 41(1), 714–725. Available from: <https://doi.org/10.1002/joc.6647>
- Oh, S.-G., Park, J.-H., Lee, S.-H. & Suh, M.-S. (2014) Assessment of the RegCM4 over East Asia and future precipitation change adapted to the RCP scenarios. *Journal of Geophysical Research: Atmospheres*, 119(6), 2913–2927. Available from: <https://doi.org/10.1002/2013JD020693>
- Oh, S.-G., Suh, M.-S. & Cha, D.-H. (2013) Impact of lateral boundary conditions on precipitation and temperature extremes over South Korea in the CORDEX regional climate simulation using RegCM4. *Asia-Pacific Journal of Atmospheric Sciences*, 49(4), 497–509. Available from: <https://doi.org/10.1007/s13143-013-0044-8>

- Oleson, K.W., Niu, G.-Y., Yang, Z.-L., Lawrence, D.M., Thornton, P. E., Lawrence, P.J. et al. (2008) Improvements to the Community Land Model and their impact on the hydrological cycle. *Journal of Geophysical Research: Biogeosciences*, 113(G1), G01021. Available from: <https://doi.org/10.1029/2007JG000563>
- Pal, J.S., Small, E.E. & Eltahir, E.A.B. (2000) Simulation of regional-scale water and energy budgets: representation of subgrid cloud and precipitation processes within RegCM. *Journal of Geophysical Research: Atmospheres*, 105(D24), 29579–29594. Available from: <https://doi.org/10.1029/2000JD900415>
- Park, C. & Min, S.-K. (2019) Multi-RCM near-term projections of summer climate extremes over East Asia. *Climate Dynamics*, 52(7), 4937–4952. Available from: <https://doi.org/10.1007/s00382-018-4425-7>
- Park, J., Kim, H., Simon Wang, S.Y., Jeong, J.-H., Lim, K.-S., LaPlante, M. et al. (2020) Intensification of the East Asian summer monsoon lifecycle based on observation and CMIP6. *Environmental Research Letters*, 15(9), 0940b9. Available from: <https://doi.org/10.1088/1748-9326/ab9b3f>
- Park, J.-H., Oh, S.-G. & Suh, M.-S. (2013) Impacts of boundary conditions on the precipitation simulation of RegCM4 in the CORDEX East Asia domain. *Journal of Geophysical Research: Atmospheres*, 118(4), 1652–1667. Available from: <https://doi.org/10.1002/jgrd.50159>
- Prein, A.F. & Gobiet, A. (2017) Impacts of uncertainties in European gridded precipitation observations on regional climate analysis. *International Journal of Climatology*, 37(1), 305–327. Available from: <https://doi.org/10.1002/joc.4706>
- Qiu, L., Im, E.-S., Hur, J. & Shim, K.-M. (2020) Added value of very high resolution climate simulations over South Korea using WRF modeling system. *Climate Dynamics*, 54(1), 173–189. Available from: <https://doi.org/10.1007/s00382-019-04992-x>
- Ratnam, J.V. & Kumar, K.K. (2005) Sensitivity of the simulated monsoons of 1987 and 1988 to convective parameterization schemes in MM5. *Journal of Climate*, 18(14), 2724–2743. Available from: <https://doi.org/10.1175/jcli3390.1>
- Reichler, T. & Kim, J. (2008) How well do coupled models simulate Today's climate? *Bulletin of the American Meteorological Society*, 89(3), 303–312. Available from: <https://doi.org/10.1175/bams-89-3-303>
- Reisner, J., Rasmussen, R.M. & Bruintjes, R.T. (1998) Explicit forecasting of supercooled liquid water in winter storms using the MM5 mesoscale model. *Quarterly Journal of the Royal Meteorological Society*, 124(548), 1071–1107. Available from: <https://doi.org/10.1002/qj.49712454804>
- Ritter, B. & Geleyn, J.-F. (1992) A comprehensive radiation scheme for numerical weather prediction models with potential applications in climate simulations. *Monthly Weather Review*, 120(2), 303–325. Available from: [https://doi.org/10.1175/1520-0493\(1992\)120<0303:Acfsfn>2.0.Co;2](https://doi.org/10.1175/1520-0493(1992)120<0303:Acfsfn>2.0.Co;2)
- Ruti, P.M., Somot, S., Giorgi, F., Dubois, C., Flaounas, E., Obermann, A. et al. (2016) Med-CORDEX initiative for Mediterranean climate studies. *Bulletin of the American Meteorological Society*, 97(7), 1187–1208. Available from: <https://doi.org/10.1175/bams-d-14-00176.1>
- Saeed, F., Hagemann, S. & Jacob, D. (2009) Impact of irrigation on the South Asian summer monsoon. *Geophysical Research Letters*, 36(20), L20711. Available from: <https://doi.org/10.1029/2009GL040625>
- Samala, B.K., Banerjee, N.C.S., Kaginalkar, A. & Dalvi, M. (2013) Study of the Indian summer monsoon using WRF–ROMS regional coupled model simulations. *Atmospheric Science Letters*, 14(1), 20–27. Available from: <https://doi.org/10.1002/asl2.409>
- Schrodin, R. & Heise, E. (2002) A new multi-layer soil-model. *COSMO Newsletter*, 2, 149–151.
- Seifert, A. & Beheng, K.D. (2001) A double-moment parameterization for simulating autoconversion, accretion and selfcollection. *Atmospheric Research*, 59–60, 265–281. Available from: [https://doi.org/10.1016/S0169-8095\(01\)00126-0](https://doi.org/10.1016/S0169-8095(01)00126-0)
- Shin, J., Lee, H.-S., Kim, M. & Kwon, W.-T. (2010) An uncertainty assessment for annual variability of precipitation simulated by AOGCMs over East Asia. *Atmosphere*, 20(2), 111–130 (in Korean with English abstract).
- Simmons, A., Uppala, S., Dee, D. & Kobayashi, S. (2007) ERA-Interim: New ECMWF reanalysis products from 1989 onwards. *ECMWF Newsletter*, 110, 25–35.
- Suhas, E. & Goswami, B.N. (2008) Regime shift in Indian summer monsoon climatological intraseasonal oscillations. *Geophysical Research Letters*, 35(20), L20703. Available from: <https://doi.org/10.1029/2008GL035511>
- Tang, J., Wang, S., Niu, X., Hui, P., Zong, P. & Wang, X. (2017) Impact of spectral nudging on regional climate simulation over CORDEX East Asia using WRF. *Climate Dynamics*, 48(7), 2339–2357. Available from: <https://doi.org/10.1007/s00382-016-3208-2>
- Tangang, F., Chung, J.X., Juneng, L., Supari, Salimun, E., Ngai, S.T. et al. (2020) Projected future changes in rainfall in Southeast Asia based on CORDEX–SEA multi-model simulations. *Climate Dynamics*, 55(5–6), 1247–1267. Available from: <https://doi.org/10.1007/s00382-020-05322-2>
- Tao, Y., Cao, J., Lan, G. & Su, Q. (2016) The zonal movement of the Indian–East Asian summer monsoon interface in relation to the land–sea thermal contrast anomaly over East Asia. *Climate Dynamics*, 46(9), 2759–2771. Available from: <https://doi.org/10.1007/s00382-015-2729-4>
- Taylor, K.E. (2001) Summarizing multiple aspects of model performance in a single diagram. *Journal of Geophysical Research: Atmospheres*, 106(D7), 7183–7192. Available from: <https://doi.org/10.1029/2000JD900719>
- Tiedtke, M. (1989) A comprehensive mass flux scheme for cumulus parameterization in large-scale models. *Monthly Weather Review*, 117(8), 1779–1800. Available from: [https://doi.org/10.1175/1520-0493\(1989\)117<1779:Acmsfs>2.0.Co;2](https://doi.org/10.1175/1520-0493(1989)117<1779:Acmsfs>2.0.Co;2)
- Torma, C., Giorgi, F. & Coppola, E. (2015) Added value of regional climate modeling over areas characterized by complex terrain—precipitation over the Alps. *Journal of Geophysical Research: Atmospheres*, 120(9), 3957–3972. Available from: <https://doi.org/10.1002/2014JD022781>
- Vega, I., Ribera, P. & Gallego, D. (2020) Characteristics of the onset, withdrawal, and breaks of the western North Pacific summer monsoon in the 1949–2014 period. *Journal of Climate*, 33(17), 7371–7389. Available from: <https://doi.org/10.1175/jcli-d-19-0734.1>
- Wang, B. & Ho, L. (2002) Rainy season of the Asian–Pacific summer monsoon. *Journal of Climate*, 15(4), 386–398. Available from: [https://doi.org/10.1175/1520-0442\(2002\)015<0386:Rsoatap>2.0.Co;2](https://doi.org/10.1175/1520-0442(2002)015<0386:Rsoatap>2.0.Co;2)

- Wang, B., Wu, R. & Lau, K.-M. (2001) Interannual variability of the Asian summer monsoon: contrasts between the Indian and the western North Pacific–East Asian monsoons. *Journal of Climate*, 14(20), 4073–4090. Available from: [https://doi.org/10.1175/1520-0442\(2001\)014<4073:ivotas>2.0.co;2](https://doi.org/10.1175/1520-0442(2001)014<4073:ivotas>2.0.co;2)
- Wang, B. & Xu, X. (1997) Northern Hemisphere summer monsoon singularities and climatological intraseasonal oscillation. *Journal of Climate*, 10(5), 1071–1085. Available from: [https://doi.org/10.1175/1520-0442\(1997\)010<1071:Nhmsmsa>2.0.Co;2](https://doi.org/10.1175/1520-0442(1997)010<1071:Nhmsmsa>2.0.Co;2)
- Wang, X., Chen, D., Pang, G., Gou, X. & Yang, M. (2021) Historical and future climates over the upper and middle reaches of the Yellow River Basin simulated by a regional climate model in CORDEX. *Climate Dynamics*, 56(9), 2749–2771. Available from: <https://doi.org/10.1007/s00382-020-05617-4>
- Wang, Z., Duan, A. & Wu, G. (2014) Impacts of boundary layer parameterization schemes and air–sea coupling on WRF simulation of the East Asian summer monsoon. *Science China Earth Sciences*, 57(7), 1480–1493. Available from: <https://doi.org/10.1007/s11430-013-4801-4>
- Wilby, R.L. & Wigley, T.M.L. (2000) Precipitation predictors for downscaling: observed and general circulation model relationships. *International Journal of Climatology*, 20(6), 641–661. Available from: [https://doi.org/10.1002/\(SICI\)1097-0088\(200005\)20:6<641::AID-JOC501>3.0.CO;2-1](https://doi.org/10.1002/(SICI)1097-0088(200005)20:6<641::AID-JOC501>3.0.CO;2-1)
- Wilson, D.R. & Ballard, S.P. (1999) A microphysically based precipitation scheme for the UK meteorological office unified model. *Quarterly Journal of the Royal Meteorological Society*, 125(557), 1607–1636. Available from: <https://doi.org/10.1002/qj.49712555707>
- Xue, Y., Janjic, Z., Dudhia, J., Vasic, R. & De Sales, F. (2014) A review on regional dynamical downscaling in intraseasonal to seasonal simulation/prediction and major factors that affect downscaling ability. *Atmospheric Research*, 147–148, 68–85. Available from: <https://doi.org/10.1016/j.atmosres.2014.05.001>
- Yan, G., Wen-Jie, D., Fu-Min, R., Zong-Ci, Z. & Jian-Bin, H. (2013) Surface air temperature simulations over China with CMIP5 and CMIP3. *Advances in Climate Change Research*, 4(3), 145–152. Available from: <https://doi.org/10.3724/SP.J.1248.2013.145>
- Yatagai, A., Kamiguchi, K., Arakawa, O., Hamada, A., Yasutomi, N. & Kitoh, A. (2012) APHRODITE: constructing a long-term daily gridded precipitation dataset for Asia based on a dense network of rain gauges. *Bulletin of the American Meteorological Society*, 93(9), 1401–1415. Available from: <https://doi.org/10.1175/bams-d-11-00122.1>
- Yu, K., Hui, P., Zhou, W. & Tang, J. (2020) Evaluation of multi-RCM high-resolution hindcast over the CORDEX East Asia Phase II region: mean, annual cycle and interannual variations. *International Journal of Climatology*, 40(4), 2134–2152. Available from: <https://doi.org/10.1002/joc.6323>
- Zhu, S., Remedio, A.R.C., Sein, D.V., Sielmann, F., Ge, F., Xu, J. et al. (2020) Added value of the regionally coupled model ROM in the East Asian summer monsoon modeling. *Theoretical and Applied Climatology*, 140(1), 375–387. Available from: <https://doi.org/10.1007/s00704-020-03093-8>
- Zou, L. & Zhou, T. (2016) Future summer precipitation changes over CORDEX-East Asia domain downscaled by a regional ocean-atmosphere coupled model: A comparison to the stand-alone RCM. *Journal of Geophysical Research: Atmospheres*, 121(6), 2691–2704. Available from: <https://doi.org/10.1002/2015jd024519>
- Zou, L. & Zhou, T. (2022) Mean and extreme precipitation changes over China under SSP scenarios: results from high-resolution dynamical downscaling for CORDEX East Asia. *Climate Dynamics*, 58(3), 1015–1031. Available from: <https://doi.org/10.1007/s00382-021-05947-x>
- Zou, L., Zhou, T. & Peng, D. (2016) Dynamical downscaling of historical climate over CORDEX East Asia domain: a comparison of regional ocean–atmosphere coupled model to stand-alone RCM simulations. *Journal of Geophysical Research: Atmospheres*, 121(4), 1442–1458. Available from: <https://doi.org/10.1002/2015JD023912>

SUPPORTING INFORMATION

Additional supporting information can be found online in the Supporting Information section at the end of this article.

How to cite this article: Seo, G.-Y., Ahn, J.-B., Cha, D.-H., Suh, M.-S., Min, S.-K., Chang, E.-C., Byun, Y.-H., & Kim, J.-U. (2023). Evaluation of multi-RCM ensembles for simulating spatiotemporal variability of Asian summer monsoon precipitation in the CORDEX-East Asia Phase 2 domain. *International Journal of Climatology*, 1–20. <https://doi.org/10.1002/joc.8054>